Acta Crystallographica Section B
Structural Science
ISSN 0108-7681

Temperature-resolved study of three $[M(M'O_4)_4(TBPO)_4]$ complexes (MM' = URe, ThRe, ThTc)

Madeleine Helliwell,[a]* David Collison,[a] Gordon H. John,[b] Iain May,[a] Mark J. Sarsfield,[a,c] Clint A. Sharrad[a] and Andrew D. Sutton[a]

[a]School of Chemistry, The University of Manchester, Manchester M13 9PL, England, [b]Centre for Radiochemistry Research, School of Chemistry, The University of Manchester, Manchester M13 9PL, England, and [c]BNFL, Sellafield, Seascale, Cumbria CA20 1PG, England

Correspondence e-mail: madeleine.helliwell@manchester.ac.uk

Received 24 February 2005
Accepted 9 November 2005

The crystal structures of the title complexes were measured at several temperatures between room temperature and 100 K. Each sample shows reversible crystal-to-crystal phase transitions as the temperature is varied. The behaviour of $[U(ReO_4)_4(TBPO)_4]$ (I) and $[Th(ReO_4)_4(TBPO)_4]$ (II) (TBPO = tri-*n*-butylphosphine oxide) is very similar; at room temperature, crystals of (I) and (II) are isostructural, with space group $I\bar{4}2m$, and reducing the temperature to 100 K causes a lowering of the space-group symmetry to C-centred cells, space groups Cc for (I) and $Cmc2_1$ for (II). The variation of lattice symmetry of $[Th(TcO_4)_4(TBPO)_4]$ (III) was found to be somewhat different, with the body-centred cubic space group, $I\bar{4}3m$, occurring at 293 K, a reduction of symmetry at 230 K to the C-centred orthorhombic space group, $Cmc2_1$, and a further transition to the primitive orthorhombic space group, $Pbc2_1$, below 215 K. Elucidation of the correct space-group symmetry and the subsequent refinement was complicated in some cases by the twinning by pseudo-merohedry that arises from the lowering of the space-group symmetry, occurring as the temperature is reduced. All three of the crystal structures determined at room temperature have high atomic displacement parameters, particularly of the ^{n}Bu groups, and (III) shows disorder of some of the O atoms. The structures in the space group $Cmc2_1$, show some disorder of ^{n}Bu groups, but are otherwise reasonably well ordered; the structures of (I) in Cc and (III) in $Pbc2_1$ are ordered, even to the ends of the alkyl chains. Inter-comparison of the structures measured below 293 K, using the program *OFIT* from the *SHELXTL* package, showed that generally, they are remarkably alike, with weighted r.m.s. deviations of the M, M' and P atoms of less than 0.1 Å, as are the 293 K structures of (I) and (II) with their low-temperature counterparts. However, the structure of (III) measured in the space group $Cmc2_1$ is significantly different from both the structure of (III) at 293 K and that found below 215 K, with weighted r.m.s. deviations of the Th, Tc and P atoms of 0.40 and 0.37 Å, respectively. An extensive network of weak intra- and intermolecular C—H···O hydrogen bonds found between the atoms of the ^{n}Bu and $[M'O_4]$ groups probably influences the packing and the overall geometry of the molecules.

1. Introduction

Research into the coordination chemistry of actinides is important for the design of the safe processing of irradiated nuclear fuel. Uranium and plutonium are separated from fission products for recovery in the PUREX process (plutonium and uranium recovery by extraction). Extraction of U and Pu is achieved using a 30% TBP/kerosene mixture (TBP = tri-*n*-butylphosphate) as the organic phase, with an approxi-

mately 3 *M* nitric acid aqueous phase, containing the majority of the fission products. However, it is well established that the fission product technetium (as $[TcO_4]^-$) follows the organic phase with indirect evidence, suggesting this anion coordinates to hexavalent $\{UO_2^{2+}\}$ and tetravalent (Pu^{4+}, Zr^{4+}) metal centres (Wilson, 1996). Technetium-99 was first identified as a fission product of uranium-238 when it was isolated in very small quantities from African pitchblende (Kenna & Kuroda, 1961). It is a β emitter ($t_{\frac{1}{2}} = 2.1 \times 10^5$ years) and has a specific activity of 6.2×10^8 Bq g^{-1}. The chemistry of technetium is similar to that of rhenium and the anions, $[TcO_4]^-$ and $[ReO_4]^-$, are closely related 'weakly coordinating anions', although much less is known about the former because of its radioactivity. $[ReO_4]^-$ is known to bind to transition elements and lanthanides (Chakravorti, 1990), but there are few crystal structures of $[ReO_4]^-$ and $[TcO_4]^-$ binding to actinides, although there is spectroscopic evidence for their existence (Bol'shakov *et al.*, 1967). Recently, we reported the isostructural crystal structures of $[UO_2(ReO_4)_2(TPPO)_3]$ and $[UO_2(TcO_4)_2(TPPO)_3]$ (TPPO = triphenylphosphine oxide), in which ReO_4^- and TcO_4^- are bound to U(VI) (John *et al.*, 2004; Sarsfield *et al.*, 2004) and the neptunyl(VI) pertechnetate complex $[(NpO_2)_2(TcO_4)_2{\cdot}3H_2O)]$ has also been reported (Fedosseev *et al.*, 2003). Here we describe the structural characterization of model complexes of pertechnetate coordinating to tetravalent actinides, namely, $[U(ReO_4)_4(TBPO)_4]$ (I), $[Th(ReO_4)_4(TBPO)_4]$ (II) and $[Th(TcO_4)_4(TBPO)_4]$ (III) (TBPO = tri-*n*-butylphosphine oxide)], which may be related to the extracted species formed in solution during the PUREX process; compound (III) is the first example of a tetravalent actinide coordinated to pertechnetate. Interestingly, all three complexes exhibit a number of temperature-resolved reversible crystal-to-crystal phase transitions, which we describe in this paper; the crystal structure of (III) at 100 K has been reported previously in Sarsfield *et al.* (2004).

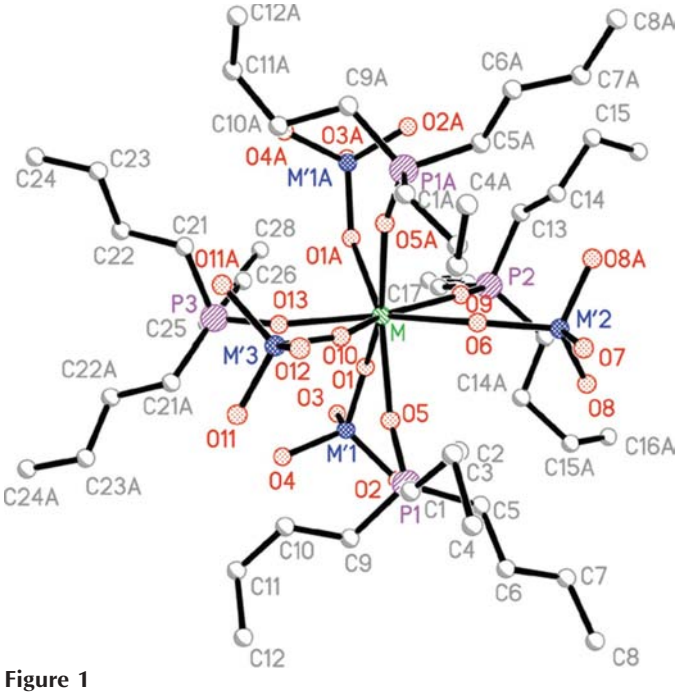

Figure 1
Ball-and-stick plot showing the numbering scheme for all the structures at 230 K and below.

2. Experimental

The synthesis and method of crystal growth for (I)–(III) have been reported previously (John, 2003; Sutton, 2003; Sarsfield *et al.* 2004).

Crystals of (I) and (II) were mounted on glass fibres, but owing to the radioactive hazard of (III) it was necessary to triply contain a crystal in a Lindemann capillary tube; triple containment involves coating the crystal in oil or epoxy resin and it is then placed in a capillary, the second layer of containment being provided by the glass of the tube. The third layer is gained by painting the capillary tube with clear nail varnish. Data were collected on a Bruker Apex CCD diffractometer (Bruker, 2001) or in one case [(I) at 100 K, §2.2.3 below] a Rigaku RAXIS IIc image-plate diffractometer, with temperature variation achieved using an Oxford Cryostream. Data processing was carried out using the *SAINT* package for the Bruker APEX data (Bruker, 2002), *DENZO* and *SCALEPACK* (Otwinowski, 1988) for the RAXIS data, and the *SHELXTL* package was used for structure solution and refinement and graphical work (Bruker, 2001). The crystal structures were solved by direct methods, unless an isostructural model was used as the starting point, and H atoms were included in calculated positions. Additional details applying to individual crystal structures are described below. Tables 1, 2 and 3 summarize the crystal data measured at the various temperatures, for (I), (II) and (III), respectively. Fig. 1 shows the numbering scheme adopted for the structures and *ORTEP* plots for each crystal structure are illustrated in Figs. 2(*a*) to (*m*).

2.1. Investigation of possible pseudo-merohedral twinning

To assess whether the lowering of the symmetry with temperature led to any pseudo-merohedral twinning, which is commonly seen in such cases (see Herbst-Irmer & Sheldrick, 1998; Parsons, 2003, for example), careful examination of the raw diffraction images was made of each of the data sets of the lower-symmetry space groups, measured at 230 K and below. This showed that some reflections were slightly split, *i.e* not into individual components, but rather into a peak with a shoulder. Evaluation trials were made increasing the box sizes (*i.e.* integration limits) by 25 and 50%, respectively, of the initially determined box size. It was, however, found that the box size optimized originally in the matrix determination from the raw images, and then during the *SAINT* data processing, had in fact led to the optimum precision in terms of the R_{int} and final R values. For instance, for the 100 K structure of (II), which showed the greatest degree of pseudo-merohedral twinning, increasing the box size by 25% led to an R_{int} of 0.0441 and a final conventional R value of 0.0339, and increasing the box size by 50% gave an R_{int} = 0.0406 and a conventional R = 0.0297. These values are both higher than

Table 1
Experimental details for (I).

	(I) at 293 K	(I) at 230 K	(I) at 165 K	(I) at 100 K
Crystal data				
Chemical formula	$C_{48}H_{108}O_{20}P_4Re_4U$	$C_{48}H_{108}O_{20}P_4Re_4U$	$C_{48}H_{108}O_{20}P_4Re_4U$	$C_{48}H_{108}O_{20}P_4Re_4U$
M_r	2112.05	2112.05	2112.05	2112.05
Cell setting, space group	Tetragonal, $I\bar{4}2m$	Orthorhombic, $Cmc2_1$	Orthorhombic, $Cmc2_1$	Monoclinic, Cc
a, b, c (Å)	15.5404 (6), 15.5404 (6), 14.8191 (11)	21.5289 (15), 21.9148 (16), 14.8288 (11)	21.4344 (15), 21.7929 (15), 14.7782 (10)	21.40 (2), 21.68 (2), 14.78 (2)
α, β, γ (°)	90.00, 90.00, 90.00	90.00, 90.00, 90.00	90.00, 90.00, 90.00	90.00, 90.00 (3), 90.00
V (Å^3)	3578.9 (3)	6996.3 (9)	6903.2 (8)	6857 (13)
Z	2	4	4	4
Dx (Mg m^{-3})	1.960	2.005	2.032	2.046
Radiation type	Mo $K\alpha$	Mo $K\alpha$	Mo $K\alpha$	Mo $K\alpha$
No. of reflections for cell parameters	3188	5703	7236	49029
θ range (°)	2.6–20.8	2.6–26.2	2.7–26.4	2.3–25.0
μ (mm^{-1})	9.14	9.35	9.48	9.55
Temperature (K)	293 (2)	230 (2)	165 (2)	100 (2)
Crystal form, colour	Block, green	Block, green	Block, green	Prismatic, green
Crystal size (mm)	0.15 × 0.15 × 0.10	0.15 × 0.15 × 0.10	0.15 × 0.15 × 0.10	0.12 × 0.1 × 0.08
Data collection				
Diffractometer	CCD area detector	CCD area detector	CCD area detector	Rigaku RAXIS
Data collection method	φ and ω scans	φ and ω scans	φ and ω scans	103 × 3° φ scans
Absorption correction	Multi-scan (based on symmetry-related measurements)	Multi-scan (based on symmetry-related measurements)	Multi-scan (based on symmetry-related measurements)	None
T_{min}	0.341	0.334	0.331	–
T_{max}	0.462	0.455	0.451	–
No. of measured, independent and observed reflections	10 483, 1941, 1699	25 273, 6529, 6180	24 887, 6428, 6171	49 029, 11 595, 11431
Criterion for observed reflections	$I > 2\sigma(I)$	$I > 2\sigma(I)$	$I > 2\sigma(I)$	$I > 2\sigma(I)$
R_{int}	0.029	0.027	0.029	0.06
θ_{max} (°)	26.4	25.0	25.0	25.0
Range of h, k, l	$-19 \Rightarrow h \Rightarrow 15$ $-17 \Rightarrow k \Rightarrow 19$ $-18 \Rightarrow l \Rightarrow 17$	$-25 \Rightarrow h \Rightarrow 25$ $-26 \Rightarrow k \Rightarrow 26$ $-17 \Rightarrow l \Rightarrow 17$	$-25 \Rightarrow h \Rightarrow 25$ $-25 \Rightarrow k \Rightarrow 25$ $-17 \Rightarrow l \Rightarrow 17$	$-25 \Rightarrow h \Rightarrow 25$ $-25 \Rightarrow k \Rightarrow 25$ $-17 \Rightarrow l \Rightarrow 17$
Refinement				
Refinement on	F^2	F^2	F^2	F^2
$R[F^2 > 2\sigma(F^2)]$, $wR(F^2)$, S	0.039, 0.099, 1.09	0.027, 0.068, 1.12	0.025, 0.065, 1.11	0.032, 0.080, 1.05
No. of reflections	1941	6529	6428	11 595
No. of parameters	102	377	417	698
H-atom treatment	Constrained to parent site	Constrained to parent site	Constrained to parent site	Constrained to parent site
Weighting scheme	$w = 1/[\sigma^2(F_o^2) + (0.0614P)^2]$, where $P = (F_o^2 + 2F_c^2)/3$	$w = 1/[\sigma^2(F_o^2) + (0.0273P)^2 + 21.6652P]$, where $P = (F_o^2 + 2F_c^2)/3$	$w = 1/[\sigma^2(F_o^2) + (0.0227P)^2 + 46.403P]$, where $P = (F_o^2 + 2F_c^2)/3$	$w = 1/[\sigma^2(F_o^2) + (0.0247P)^2 + 70.409P]$, where $P = (F_o^2 + 2F_c^2)/3$
$(\Delta/\sigma)_{max}$	0.001	0.002	0.007	0.001
$\Delta\rho_{max}$, $\Delta\rho_{min}$ (e Å^{-3})	1.03, −0.38	2.23, −1.05	2.33, −1.21	1.77, −1.87
Extinction method	None	None	None	*SHELXL*
Extinction coefficient	–	–	–	0.000349 (19)
Absolute structure	Flack (1983)	Flack (1983)	Flack (1983)	Flack (1983)
Flack parameter	0.03 (2)	0.025 (9)	0.020 (9)	0

those obtained by the normal *SAINT* data reduction procedures which gave an $R_{int} = 0.0336$ and a conventional R value of 0.0268, presumably because when the box size was increased too much background was being included with the peak. Similar results were obtained for the other low-temperature crystal structures and therefore normal data processing procedures, with optimized box sizes, were adopted for all the data sets measured using the Bruker APEX diffractometer. For the crystal structure of (I) at 100 K, measured on the RAXIS II, the box size was chosen manually to fully encompass the reflections, during the *DENZO* data processing.

In some cases the application of more than one twin law might in theory be necessary for the possible monoclinic space groups and tests were made, for data collected using the Bruker APEX diffractometer, using the program *TWINABS* (Sheldrick, 2002), which allows the application of multiple twin laws; the treatment adopted for each compound is described fully in the supplementary information[1] and the results are summarized here.

[1] Supplementary data for this paper are available from the IUCr electronic archives (Reference: WS5025). Services for accessing these data are described at the back of the journal.

Table 2
Experimental details for (II).

	(II) at 293 K	(II) at 230 K	(II) at 165 K	(II) at 100 K
Crystal data				
Chemical formula	$C_{48}H_{108}O_{20}P_4Re_4Th$	$C_{48}H_{108}O_{20}P_4Re_4Th$	$C_{48}H_{108}O_{20}P_4Re_4Th$	$C_{48}H_{108}O_{20}P_4Re_4Th$
M_r	2106.06	2106.06	2106.06	2106.06
Cell setting, space group	Tetragonal, $I\bar{4}2m$	Orthorhombic, $Cmc2_1$	Orthorhombic, $Cmc2_1$	Orthorhombic, $Cmc2_1$
a, b, c (Å)	15.5577 (12), 15.5577 (12), 14.8730 (17)	21.721 (3), 21.738 (3), 14.8793 (19)	21.610 (3), 21.623 (3), 14.8324 (19)	21.535 (3), 21.548 (3), 14.7950 (19)
α, β, γ (°)	90.00, 90.00, 90.00	90.00, 90.00, 90.00	90.00, 90.00, 90.00	90.00, 90.00, 90.00
V (Å^3)	3599.9 (6)	7025.4 (16)	6930.7 (15)	6865.4 (15)
Z	2	4	4	4
D_x (Mg m^{-3})	1.943	1.991	2.018	2.038
Radiation type	Mo $K\alpha$	Mo $K\alpha$	Mo $K\alpha$	Mo $K\alpha$
No. of reflections for cell parameters	1544	5355	5437	8488
θ range (°)	2.7–20.5	2.6–23.0	2.7–25.9	2.7–26.5
μ (mm^{-1})	8.91	9.13	9.25	9.34
Temperature (K)	293 (2)	230 (2)	165 (2)	100 (2)
Crystal form, colour	Plate, colourless	Plate, colourless	Plate, colourless	Block, colourless
Crystal size (mm)	0.18 × 0.18 × 0.10	0.18 × 0.18 × 0.10	0.18 × 0.18 × 0.10	0.18 × 0.18 × 0.10
Data collection				
Diffractometer	CCD area detector	CCD area detector	CCD area detector	CCD area detector
Data collection method	φ and ω scans	φ and ω scans	φ and ω scans	φ and ω scans
Absorption correction	Multi-scan (based on symmetry-related measurements)	Multi-scan (based on symmetry-related measurements)	Multi-scan (based on symmetry-related measurements)	Multi-scan (based on symmetry-related measurements)
T_{min}	0.297	0.290	0.689	0.284
T_{max}	0.470	0.462	1.000	0.455
No. of measured, independent and observed reflections	5728, 1932, 1605	18 098, 6391, 6029	24 808, 6458, 6367	24 358, 6390, 6376
Criterion for observed reflections	$I > 2\sigma(I)$	$I > 2\sigma(I)$	$I > 2\sigma(I)$	$I > 2\sigma(I)$
R_{int}	0.028	0.042	0.036	0.034
θ_{max} (°)	26.4	25.0	25.0	25.0
Range of h, k, l	$-19 \Rightarrow h \Rightarrow 7$ $-12 \Rightarrow k \Rightarrow 16$ $-16 \Rightarrow l \Rightarrow 18$	$-25 \Rightarrow h \Rightarrow 25$ $-12 \Rightarrow k \Rightarrow 25$ $-16 \Rightarrow l \Rightarrow 17$	$-25 \Rightarrow h \Rightarrow 25$ $-25 \Rightarrow k \Rightarrow 25$ $-17 \Rightarrow l \Rightarrow 17$	$-25 \Rightarrow h \Rightarrow 25$ $-25 \Rightarrow k \Rightarrow 25$ $-17 \Rightarrow l \Rightarrow 17$
Refinement				
Refinement on	F^2	F^2	F^2	F^2
$R[F^2 > 2\sigma(F^2)]$, $wR(F^2)$, S	0.044, 0.117, 1.01	0.036, 0.076, 1.07	0.026, 0.054, 1.06	0.027, 0.059, 1.16
No. of reflections	1932	6391	6458	6390
No. of parameters	102	393	372	393
H-atom treatment	Constrained to parent site	Constrained to parent site	Constrained to parent site	Constrained to parent site
Weighting scheme	w = $1/[\sigma^2(F_o^2) + (0.0736P)^2]$, where $P = (F_o^2 + 2F_c^2)/3$	$w = 1/[\sigma^2(F_o^2) + (0.0314P)^2 + 8.8462P]$, where $P = (F_o^2 + 2F_c^2)/3$	$w = 1/[\sigma^2(F_o^2) + (0.0201P)^2 + 25.4516P]$, where $P = (F_o^2 + 2F_c^2)/3$	$w = 1/[\sigma^2(F_o^2) + (0.0121P)^2 + 76.2392P]$, where $P = (F_o^2 + 2F_c^2)/3$
(Δ/σ)max	<0.0001	<0.0001	0.002	0.002
$\Delta\rho_{max}$, $\Delta\rho_{min}$ (e Å^{-3})	0.79, −0.59	1.13, −1.55	1.10, −1.05	1.62, −1.34
Extinction method	None	None	None	None
Absolute structure	Flack (1983)	Flack (1983)	Flack (1983)	Flack (1983)
Flack parameter	0.09 (4)	0.037 (15)	0.011 (11)	0.027 (13)

Each compound showed a reduction of symmetry at 230 K. The lattice type became primitive owing to a doubling of the number of diffraction spots and although the cell dimensions were still similar, the crystals were no longer tetragonal; the primitive unit cells could be transformed to C-centred lattices. Three space-group choices were possible, either $Cmc2_1$ or Cc in the C-centred lattice or $P2_1$ in the primitive lattice. Refinement in $Cmc2_1$ was carried out using the twin law (0 1 0/ 1 0 0/ 0 0 −1) to account for the possible pseudo-merohedral twinning arising from the fact that the metric symmetry of the unit cells, which appears to be tetragonal due to the similarity of a and b, was higher than the symmetry of the structures. However, although the agreement factors for each structure refined in the space group $Cmc2_1$ were excellent (see Tables 1, 2 and 3), there was disorder seen in the ^{n}Bu group C13–C16, and for the atom C25. Therefore, the space groups Cc and $P2_1$ were also investigated to see whether by lowering the symmetry still further, this disorder could be removed.

For the space group Cc, because the metric symmetry was approximately tetragonal, but the symmetry to be tested was monoclinic, to fully deal with possible pseudo-merohedral twinning, the twin laws (0 1 0/1 0 0/0 0 −1), (1 0 0/0 −1 0/0 0 −1) and (0 1 0/−1 0 0/0 0 1), together with inversion twinning for each domain might, in theory, all be necessary. Likewise, for the space group $P2_1$, the possible twin laws are (1 0 0/0 −1 0/0 0 −1), (0 0 1/0 −1 0/1 0 0) and (0 0 1/0 1 0/−1 0 0), together

Table 3
Experimental details for (III).

	(III) at 293 K	(III) at 230 K	(III) at 170 K	(III) at 130 K	(III) at 100 K
Crystal data					
Chemical formula	$C_{48}H_{108}O_{20}P_4Tc_4Th$	$C_{48}H_{108}O_{20}P_4Tc_4Th$	$C_{48}H_{108}O_{20}P_4Tc_4Th$	$C_{48}H_{108}O_{20}P_4Tc_4Th$	$C_{48}H_{108}O_{20}P_4Tc_4Th$
M_r	1753.26	1753.26	1753.26	1753.26	1753.26
Cell setting, space group	Cubic, $I\bar{4}3m$	Orthorhombic, $Cmc2_1$	Orthorhombic, $Pbc2_1$	Orthorhombic, $Pbc2_1$	Orthorhombic, $Pbc2_1$
a, b, c (Å)	15.3423 (10), 15.3423 (10), 15.3423 (10)	21.444 (2), 21.582 (2), 14.736 (2)	21.417 (6), 21.649 (6), 14.848 (4)	21.358 (13), 21.651 (13), 14.790 (9)	21.386 (4), 21.732 (4), 14.820 (2)
α, β, γ (°)	90.00, 90.00, 90.00	90.00, 90.00, 90.00	90.00, 90.00, 90.00	90.00, 90.00, 90.00	90.00, 90.00, 90.00
V (Å^3)	3611.4 (4)	6819.9 (13)	6885 (3)	6839 (7)	6888 (2)
Z	2	4	4	4	4
D_x (Mg m^{-3})	1.612	1.708	1.692	1.703	1.691
Radiation type	Mo $K\alpha$	Mo $K\alpha$	Mo $K\alpha$	Mo $K\alpha$	Mo $K\alpha$
No. of reflections for cell parameters	1959	5437	7727	5490	5577
θ range (°)	2.6–20.0	2.7–25.9	2.7–26.3	2.7–26.1	2.3–26.4
μ (mm^{-1})	2.95	3.12	3.09	3.11	3.09
Temperature (K)	293 (2)	230 (2)	170 (2)	130 (2)	100 (2)
Crystal form, colour	Prism, colourless	Block, colourless	Block, colourless	Block, colourless	Block, colourless
Crystal size (mm)	0.10 × 0.10 × 0.10	0.10 × 0.10 × 0.10	0.10 × 0.10 × 0.10	0.10 × 0.10 × 0.10	0.10 × 0.10 × 0.10
Data collection					
Diffractometer	CCD area detector	CCD area detector	CCD area detector	CCD area detector	CCD area detector
Data collection method	φ and ω scans	φ and ω scans	φ and ω scans	φ and ω scans	φ and ω scans
Absorption correction	None	Multi-scan (based on symmetry-related measurements)	Multi-scan (based on symmetry-related measurements)	Multi-scan (based on symmetry-related measurements)	Multi-scan (based on symmetry-related measurements)
T_{min}	–	0.746	0.748	0.746	0.748
T_{max}	–	0.746	0.748	0.746	0.748
No. of measured, independent and observed reflections	6235, 723, 651	26 789, 7255, 6041	54 013, 14 267, 12 482	50 705, 14 038, 12 090	35 481, 13 901, 12 000
Criterion for observed reflections	$I > 2\sigma(I)$	$I > 2\sigma(I)$	$I > 2\sigma(I)$	$I > 2\sigma(I)$	$I > 2\sigma(I)$
R_{int}	0.041	0.055	0.074	0.090	0.073
θ_{max} (°)	26.3	26.5	26.5	26.4	26.6
Range of h, k, l	$-12 \Rightarrow h \Rightarrow 18$ $-3 \Rightarrow k \Rightarrow 19$ $-19 \Rightarrow l \Rightarrow 18$	$-26 \Rightarrow h \Rightarrow 26$ $-26 \Rightarrow k \Rightarrow 26$ $-17 \Rightarrow l \Rightarrow 18$	$-26 \Rightarrow h \Rightarrow 26$ $-27 \Rightarrow k \Rightarrow 27$ $-18 \Rightarrow l \Rightarrow 18$	$-26 \Rightarrow h \Rightarrow 26$ $-26 \Rightarrow k \Rightarrow 26$ $-17 \Rightarrow l \Rightarrow 18$	$-25 \Rightarrow h \Rightarrow 26$ $-25 \Rightarrow k \Rightarrow 27$ $-18 \Rightarrow l \Rightarrow 18$
Refinement					
Refinement on	F^2	F^2	F^2	F^2	F^2
$R[F^2 > 2\sigma(F^2)]$, $wR(F^2)$, S	0.039, 0.101, 1.01	0.037, 0.088, 0.97	0.050, 0.127, 1.08	0.053, 0.130, 1.05	0.062, 0.161, 1.09
No. of reflections	723	7255	14 267	14 038	13 901
No. of parameters	50	354	707	707	707
H-atom treatment	Constrained to parent site	Constrained to parent site	Constrained to parent site	Constrained to parent site	Constrained to parent site
Weighting scheme	$w = 1/[\sigma^2(F_o^2) + (0.0666P)^2]$, where $P = (F_o^2 + 2F_c^2)/3$	$w = 1/[\sigma^2(F_o^2) + (0.0428P)^2]$, where $P = (F_o^2 + 2F_c^2)/3$	$w = 1/[\sigma^2(F_o^2) + (0.042P)^2 + 14.969P]$, where $P = (F_o^2 + 2F_c^2)/3$	$w = 1/[\sigma^2(F_o^2) + (0.0001P)^2 + 21.3104P]$, where $P = (F_o^2 + 2F_c^2)/3$	$w = 1/[\sigma^2(F_o^2) + (0.0606P)^2 + 22.3563P]$, where $P = (F_o^2 + 2F_c^2)/3$
$(\Delta\sigma)_{max}$	0.002	0.004	0.002	0.004	0.003
$\Delta\rho_{max}$, $\Delta\rho_{min}$ (e Å^{-3})	0.63, −0.27	1.43, −0.77	3.57, −0.88	3.15, −1.14	4.83, −3.49
Extinction method	None	None	None	None	None
Absolute structure	Flack (1983)	Flack (1983)	Flack (1983)	Flack (1983)	Flack (1983)
Flack parameter	0.00 (2)	0.034 (7)	0.016 (6)	0.017 (6)	0.020 (8)

Computer programs used: Bruker *SMART* (Bruker, 2001), *MSC RAXIS*11 Control, *DENZO* (Otwinowski, 1988), *SAINT* (Bruker, 2002), *SHELXS*97 (Sheldrick, 1997), *SIR*97 (Altomare *et al.* 1999), *SHELXL*97 (Sheldrick, 1997), *SHELXTL*, *TEXSAN* (Molecular Structure Corporation, 1995).

with inversion twinning for each domain. Therefore, for each structure which could be refined in the space group $Cmc2_1$, the lower-symmetry space groups Cc and $P2_1$ were also investigated, with the application of the multiple twin laws using the program *TWINABS* (Sheldrick, 2002). The treatment used for each compound, at each possible temperature, is fully described in the supplementary information and the final choice of space groups is discussed in §3.1. However, in summary, for (I), the space group $Cmc2_1$ was found to be best for all temperatures from 230 K and below, except for the RAXIS II data measured at 100 K, for which Cc gave the optimal results. Also, there was essentially no twinning

observed for the structures of (I) in $Cmc2_1$. There was, however, a degree of twinning for the structure of (I) in *Cc*, arising from the orthorhombic metric symmetry, but monoclinic symmetry of the structure; the extent of this twinning was *ca* 14% and the twin law used to account for it was (1 0 0/0 −1 0/0 0 −1). For (II), the space group $Cmc2_1$ was optimal for all the structures at 230 K and below, including that at 100 K; for this sample a high degree of pseudo-merohedral twinning (twin fraction, approximately 50%) was observed at each of the temperatures, arising from the fact that the metric symmetry was approximately tetragonal, but the symmetry of the structure was orthorhombic [twin law (0 1 0/ 1 0 0/ 0 0 −1)]; for (III), the space group at 230 K was found to be $Cmc2_1$, rather than *Cc* or $P2_1$, and a much lower degree of pseudo-merohedral twinning [twin law (0 1 0/ 1 0 0/ 0 0 −1)] was observed than for (II), of 17.4 (1)%. At lower temperatures, the space-group symmetry of (III) was $Pbc2_1$ and the twin fraction refined to values between *ca* 7 and 8%.

Therefore, in all cases it was possible to describe the twinning using a single twin law in the instruction file, with in one case [(I) at 100 K], additional racemic twinning. That the twinning is suitably explained using a single twin law is also indicated by the precision of the structures, in terms of the excellent *R* values, the stability of the refinements and the fact that the geometry was reasonable.

Further details about all the refinements for (I), (II) and (III) are reported in the experimental details below (§§2.2–2.4) and the choice of space groups is discussed in §3.1.

2.2. $[U(ReO_4)_4(TBPO)_4]$ (I)

2.2.1. 293 K. An initial structure solution located the U, Re and O atoms. The C atoms of the ^{n}Bu groups were then found by successive difference-Fourier cycling techniques; their thermal motion is very high and restraints were used on their bond lengths and angles. The non-H atoms were refined anisotropically, with restraints applied to those of the ^{n}Bu C atoms.

2.2.2. 230 and 165 K. The structures, which were found to be in the space group $Cmc2_1$ (see above and the supplementary information) are isostructural with (III), measured at 230 K (see §2.4.2), whose structure was used as a starting point, and a similar refinement method was used. Tests were made to determine whether the crystal was twinned with the twin matrix (0 1 0/1 0 0/0 0 −1); the twin fraction refined to values of 0.0131 (4) and 0.0200 (4) for the 230 and 165 K structures, respectively. These refined values showed that there was essentially no twinning seen for the structures of (I) in the space group $Cmc2_1$. C25 is disordered, with the other component related by mirror symmetry; the ^{n}Bu group, C13–C16, is disordered over two sites, whose occupancy was constrained to sum to 1.0.

2.2.3. 100 K. The data were collected using the RAXIS in 105 × 3° phi oscillations of 10 min per exposure on a Mo $K\alpha$ Rigaku rotating-anode generator. The crystal was a racemic twin, as well as having twinning arising from the approximate 90° β angle. The extent of the latter twinning was ∼ 13.8 (9)% and the matrix employed to account for this was (1 0 0/0 −1 0/ 0 0 −1); the application of the twin law reduced the *R* value from 0.0418 to 0.0321. Clearly, there might have been additional twinning arising from the similarity of *a* and *b*, but with the excellent precision, stability of the refinement and lack of the need for restraints on the parameters, it was assumed that the single twin matrix, with account taken of the additional racemic twinning was sufficient to describe the situation properly. Moreover, this corresponds with the lack of such twinning found in the 230 and 165 K crystal structures (see above and the supplementary information).

2.3. $[Th(ReO_4)_4(TBPO)_4]$ (II)

2.3.1. 293 K. The model for the 293 K structure of (I) (the isostructural U/Re equivalent) was used as a starting point and the refinement details are as described above (§2.2.1).

2.3.2. 230 and 165 K. The structures are isostructural with (III), measured at 230 K, *i.e.* in space group $Cmc2_1$ (see the supplementary information and §3.1 for a full discussion of the choice of space group), whose parameters were used initially and the refinement details and patterns of disorder are similar (see §2.4.2). The crystal was twinned such that the twin matrix was (0 1 0/ 1 0 0/ 0 0 −1) and the twin fraction refined to similar values of 0.478 (1) and 0.489 (1) for the 230 and 165 K structures, respectively; without the application of the twin matrix, the refinement of the structure was unstable and the *R* values were around 0.19, whereas introducing the twin law reduced the *R* values to 0.0398 and 0.0260, respectively, and led to stable refinements. As is often the case with a high degree of twinning, some restraints of the geometric parameters of the ^{n}Bu groups, as well as the anisotropic thermal parameters, was required (Herbst-Irmer & Sheldrick, 1998).

2.3.3. 100 K. The structure is isostructural with that of (II) measured at 165 K and the refined model was used as a starting point (see supplementary information and §3.1 for a full discussion of the choice of space group). The crystal was twinned with the twin matrix (0 1 0/ 1 0 0/ 0 0 −1) and the twin fraction refined to 0.496 (1). As in the case of the 230 and 165 K structures of (II), the application of the twin law was essential in providing a stable refinement, with an excellent final *R* value of 0.0268. Further details of the structure refinement are the same as in §2.3.2.

2.4. $[Th(TcO_4)_4(TBPO)_4]$ (III)

2.4.1. 293 K. Non-H atoms were refined anisotropically, with restraints on the a.d.p.s of the O and C atoms and the geometry of the ^{n}Bu group. The O atoms bonded to Th are disordered over three sites, related by space-group symmetry; this disorder was not removed when the symmetry was lowered.

2.4.2. 230 K. The space group was found to be $Cmc2_1$ (see supplementary information and §3.1 for a full discussion of the choice of space group). The crystal was twinned such that the twin matrix was (0 1 0/1 0 0/0 0 −1) and the twin fraction refined to a value of 0.174 (1); the introduction of the twin law to the refinement significantly reduced the *R* value from

0.0557 to 0.0373. The asymmetric unit contains $\frac{1}{2}$ of the molecule. C25 is disordered over two sites related by mirror symmetry. C13 is also disordered over two sites whose occupancies were constrained to sum to unity. Restraints were applied to the bond lengths and angles of some of the atoms of the ^{n}Bu groups. The non-H atoms, except the disordered C atoms, were refined anisotropically, using restraints for those of the partially occupied C atoms.

2.4.3. 170, 130 and 100 K. Initially, the crystal structure was solved by direct methods in the space group $Pbc2_1$, then

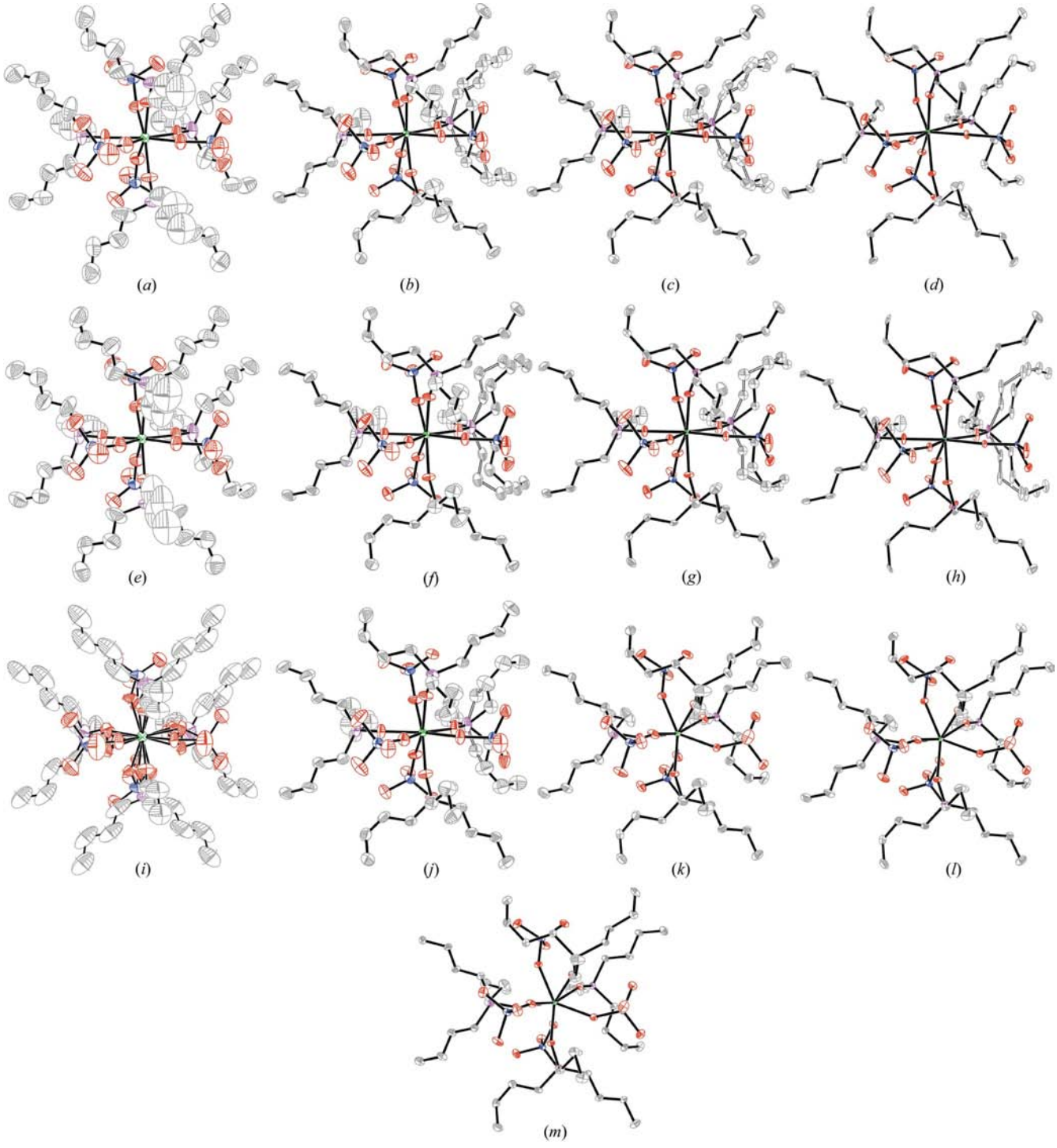

Figure 2
Plots of (I), (II) and (III) with H atoms omitted for clarity. The same view has been used for all plots to allow comparison of the structures. For (I) M = U and M' = Re, for (II) M = Th and M' = Re and for (III) M = Th and M' = Tc. *ORTEP* plots are with 30% probablility displacement ellipsoids. (*a*) (I) at 293 K; (*b*) (I) at 230 K; (*c*) (I) at 165 K; (*d*) (I) at 100 K; (*e*) (II) at 293 K; (*f*) (II) at 230 K; (*g*) (II) at 165 K; (*h*) (II) at 100 K; (*i*) (III) at 293 K; (*j*) (III) at 230 K; (*k*) (III) at 170 K; (*l*) (III) at 130 K; (*m*) (III) at 100 K.

having verified that this indeed was the correct space-group symmetry, the expanded structure solution at 230 K was used as a starting point with the origin shifted by 0.25 −0.25 −0.15. This was to obtain an equivalent numbering scheme in the lower symmetry for ease of comparison of the structures with the higher temperature structures in the space group $Cmc2_1$. The structures obtained by direct solution and by expansion and shifting of the origin were exactly equivalent. The crystal was twinned such that the twin matrix was (0 1 0/ 1 0 0/ 0 0 −1) and the twin fractions refined to values of 0.088 (1), 0.071 (1) and 0.073 (1), respectively. A few restraints were applied to the bond lengths and angles of the atoms of the ^{n}Bu groups.

2.5. Determination of C—H hydrogen bonds

An extensive network of possible weak intra- and intermolecular C—H···O hydrogen bonds was found between the C atoms of the ^{n}Bu groups and the O atoms of the [$M'O_4$] groups. The H-atom positions were calculated and are reasonably certain, except for those of the methyl groups; for these H atoms, it was necessary to calculate the H-atom positions to provide a staggered conformation with respect to the bonding CH_2, rather than from the torsion angle that maximized the electron density. The latter method is preferable, particularly for hydrogen-bond determination, since it allows the optimum positioning of the methyl H atoms, but was not possible in this study because the H-atom electron density was masked by that from the heavy atoms. *PARST*, from the *WinGX* system (*PARST*, Nardelli, 1995; *WinGX*, Farrugia, 1999) was used to determine the C—H hydrogen bonds for distances between the donor C atom and the acceptor O atom of less than 4 Å. These hydrogen bonds were then included in the *SHELXL*97 refinement for the structures measured at 230 and 100 K.

3. Results

3.1. Thermotropic phase transitions

3.1.1. (I) and (II). At 293 and 260 K, (I) and (II) crystallize in the body-centred tetragonal space group $I\bar{4}2m$ and the asymmetric unit contains 1/8 of the molecule. The M atom [M = U for (I) and Th for (II)] lies on a special position ($\bar{4}2m$) and also a number of the atoms lie on a mirror plane. Plots of the 293 K structures of (I) and (II) are shown in Figs. 2(*a*) and (*e*), which indicate the very high a.d.p.s, particularly of the ^{n}Bu groups. A number of lower symmetry space groups were investigated, but reducing the symmetry did not lead to an improved structural model.

Reducing the temperature to 230 K, however, did lead to a striking improvement, not just by virtue of the temperature change but also due to a change in lattice symmetry. This was manifested by a doubling of the number of diffraction spots, arising from the removal of body-centering (see Figs. 3*a* and *b*), to give a primitive unit cell of similar dimensions to that at 293 K; the primitive lattice could be transformed to a C-centred lattice. The merging R factor of 0.277 for the diffraction intensities for the crystal of (I) clearly indicated that the lattice was no longer tetragonal, but instead was either C-centred orthorhombic, monoclinic or primitive monoclinic, space groups $Cmc2_1$, Cc or $P2_1$, respectively (the latter space group using the primitive setting of the unit cell prior to transformation to the C-centred lattice); all three space groups were tried and a detailed description of the investigation and handling of possible pseudo-merohedral twinning for the possible monoclinic space groups is described in the supplementary information and summarized in §2. Eventually, the space group $Cmc2_1$ was selected as the most satisfactory for the final refinement, for a number of reasons; firstly, the solution in $P2_1$ showed the same patterns of high a.d.p.s or disorder as were observed in $Cmc2_1$, and in fact in many cases, the thermal ellipsoids were found to be more eccentric; the conventional R value was also higher, at 0.032 (*versus* 0.027), although the R_{int} values were very similar at 0.024 and 0.027, for $P2_1$ and $Cmc2_1$, respectively. For Cc the conventional R factor was 0.028 and the R_{int} was 0.023, but there were problems with the a.d.p.s of the C and O atoms, including a non-positive definite C atom. Finally, the C—C bond length precision was best in the space group $Cmc2_1$ at 0.018 Å (*versus* 0.021 and 0.028 Å for $P2_1$ and Cc, respectively). The final structure in $Cmc2_1$ is shown in Fig. 2(*b*).

The choice of space group for (II) at 230 K was complicated still further by the fact that the merging R value suggested that the lattice symmetry was primitive tetragonal; a number of space groups were tried, but it became clear that the symmetry was lower, as for (I); again the space groups $Cmc2_1$, Cc and $P2_1$ were all tested, but for analogous reasons as for (I), $Cmc2_1$ was finally selected as the optimum (see the supplementary information for a detailed description of the investigation and handling of possible pseudo-merohedral twinning for the possible monoclinic space groups); the structure is shown in Fig. 2(*f*). In this case the degree of pseudo-merohedral twinning with the twin law (0 1 0/ 1 0 / 0 0 −1) was found to be very high at 47.8 (1)%, probably because the a and b unit-cell parameters are much more similar than for (I), where essentially no such twinning was seen (§2). The high degree of twinning explains the apparent tetragonal symmetry of the diffraction pattern (Herbst-Irmer & Sheldrick 1998; Parsons, 2003). The space group of the crystal structures of (I) and (II), measured at 165 K, were also deduced to be $Cmc2_1$ after trials in all three possible space groups; plots are shown in Fig. 2(*c*) and (*g*).

Somewhat ambiguous results were obtained for (I) at 100 K; data collection was originally carried out using the RAXIS 11 image-plate diffractometer, and again structure solution and refinement were carried out in the space groups $Cmc2_1$, Cc and $P2_1$. Both the $P2_1$ and $Cmc2_1$ groups were discounted, owing to the presence of regions of disorder and/or non-positive definite thermal parameters not present in Cc. Moreover, refinement in the space group Cc was possible without any restraints on the geometry or the thermal parameters, in contrast to refinement in $P2_1$ and $Cmc2_1$, and the structure was well ordered, even to the ends of the ^{n}Bu groups. The R value was also better in Cc than in $P2_1$ and $Cmc2_1$ (0.032 *versus* 0.041 and 0.037, respectively). Thus, on balance, the

space group *Cc* was preferred for the final refinement, using this particular data set, and the structure is plotted in Fig. 2(*d*). Later, a further set of data on a different crystal was collected at 100 K, using the Bruker APEX CCD diffractometer; this time, the space group $Cmc2_1$ seemed to be superior, since the disordered regions were not improved significantly by reducing the symmetry and, moreover, *ADDSYM* (from *PLATON*; Spek, 2003) detected additional symmetry suggesting $Cmc2_1$ for both the monoclinic space groups. Possible explanations for the differing result in the later experiment are firstly that the transition to *Cc* occurs close to 100 K and perhaps the crystal was better positioned in the cold stream in the RAXIS experiment, and therefore the crystal was kept at a slightly lower temperature during the data collection; another possibility is that there is some variation in behaviour from crystal to crystal. A further possibility is that the rate of cooling to the data-collection temperature might lead to different behaviour; for the RAXIS II data collection, flash cooling was used to cool the crystal to 100 K; for data collection using the Bruker APEX diffractometer, three data sets were collected at 100 K involving both flash cooling and more gradual cooling to the desired temperature, but similar results were obtained for each of the 100 K Bruker APEX data sets. A data collection at 95 K was carried out, but since the cryostream is at its limit at this temperature, the temperature was not as stable as usual, varying by about a degree. However, there were signs that some adjustment towards *Cc* had occurred at this temperature; the atoms particularly affected by the lowering of symmetry are those of the disordered ^{n}Bu group (C13–C16) and C25 (see Fig. 1), which is disordered in $Cmc2_1$ because it is removed slightly from the mirror plane, on which the other atoms of that ^{n}Bu lie (C26–C28). Of the heavier atoms, P2, O7 and O11 have higher and more eccentric a.d.p.s than the average for atoms of the same type, in $Cmc2_1$. If the reduction of symmetry to *Cc* leads to a reduction of the a.d.p.s of these atoms in particular, then this is a sign of the transition towards the space group *Cc*. This was clearly seen for the data measured using the RAXIS 11*c* at 100 K; for the data measured at 95 K on the Bruker APEX, there is no great difference between the a.d.p.s of the P and O atoms, but there are indications of improvement for some of the C atoms. Firstly, C13–C16 could be refined anisotropically, without the need to split the atoms into disordered components; secondly, C25–C28 are reasonably well ordered in *Cc*, whereas in $Cmc2_1$, C25 is (as always) disordered and C26–C28 show such eccentric a.d.p.s that it was suggested in the *SHELXL* list file that they should be split into two components. However, the conventional *R* value was marginally better for the $Cmc2_1$ refinement than for *Cc* (0.036 *versus* 0.039) and *ADDSYM* detected the possible higher symmetry of $Cmc2_1$. Thus, the choice of space group was not clear-cut and one would therefore probably select the higher-symmetry space group. Ideally, further data collection using helium cryocooling to achieve a significantly lower temperature would resolve this issue and the authors are seeking to carry out such experiments. In addition, differential scanning calorimetry (DSC) measurements would allow the temperature of the transition to the space group *Cc* to be measured precisely and again a suitable apparatus is being sought in order to carry out these further investigations.

For (II) at 100 K, the situation was straightforward; those atoms which were disordered or showed high thermal motion in $Cmc2_1$, showed the same patterns in *Cc*, *ADDSYM* detected higher symmetry and the *R* value in $Cmc2_1$ was significantly better than it was in *Cc* (0.027 *versus* 0.031). Note that refinement in *Cc* was carried out using a single twin law, (0 1 0/ 1 0 0/ 0 0 −1). Extensive tests of the possible additional twin laws arising from the fact that the metric symmetry is tetragonal, but the structure is monoclinic, are described in §2 and the supplementary information. These showed that the application of additional twin laws led to less satisfactory and less stable refinements, thus indicating that the application of a single twin law was appropriate. The refined structure in $Cmc2_1$ is plotted in Fig. 2(*h*). However, it seems very likely that further reduction of the temperature would lead to a transition to *Cc*, since the behaviour of (II) is so similar to that of (I) and a suitable location to carry out further experiments to investigate this is being sought.

3.1.2. (III). Complex (III), $[Th(TcO_4)_4(TBPO)_4]$, crystallizes in the body-centred cubic space group $I\bar{4}3m$ at 293 K, with the Th atom lying on the $\bar{4}3m$ special position and the asymmetric unit consisting of 1/24 of the molecule, Fig. 2(*i*). In this structure, not only do the ^{n}Bu groups show extremely high thermal motion, but the O atoms linking the Th and Tc atoms, and the Th and P atoms are disordered over three sites about a 3*m* axis. Again, a number of lower symmetry space groups were tested to see if this disorder could be removed, but to no avail. The body-centred cubic space group was also seen at 260 K, but by 230 K the body centring was no longer present, as was very apparent by the number of diffraction spots doubling and the unit cell becoming primitive (Figs. 3*c* and *d*). As for (I) and (II), this primitive cell transformed to a *C*-centred cell, with possible space groups $Cmc2_1$, *Cc* or $P2_1$, the latter using the primitive setting of the unit cell. Refinement was tried first in $P2_1$, but ADDSYM indicated that this model could be converted to $Cmc2_1$, which in fact led to a more satisfactory refinement. *Cc* was also tried, but the *R* value was higher (0.052 *versus* 0.037) and there were problems with the thermal parameters, so that as for (I) and (II) the space group $Cmc2_1$ was clearly the most acceptable at a temperature of 230 K (Fig. 2*j*). Note that *TWINABS* (Sheldrick, 2002) was used to investigate the application of the multiple twin laws, which might be possible in the monoclinic space groups owing to the fact that the metric symmetry is close to tetragonal and these trials are described in the supplementary information and summarized in §2; however, this did not change the conclusion that the orthorhombic space group was the correct choice. Moreover, a further transition to the space group $Pbc2_1$ takes place below 215 K (described in the next paragraph), which can be rationalized because it is a maximal subgroup of $Cmc2_1$; in contrast, the space group $Pbc2_1$ is not a maximal subgroup of $P2_1$ or *Cc* and a possible transition from one of these monoclinic space groups to $Pbc2_1$ would instead

represent an increase in symmetry at the lower temperature rather than a decrease, and would therefore be unlikely.

Further reduction of the temperature below 230 K was carried out, and by 205 K the space group $Cmc2_1$ no longer gave an adequate refinement. The R value was higher and increased thermal motion was observed for the Tc, P and O atoms. $P2_1$ did not give an improved solution, but the solution in Cc was better although still showed some problems with not only the a.d.p.s, but also the geometry, initially thought to arise from twinning. Eventually, it became clear, once the temperature was lowered still further, that the number of diffraction spots had again doubled, as shown in Fig. 3(*e*) (*i.e.* quadrupled overall *versus* the 293 K diffraction pattern), marking a transition to a primitive unit cell of similar dimensions to the C centred cell, and the space group was found to be $Pbc2_1$ (a non-standard setting of $Pca2_1$, used here for ease of comparison with the other crystal structures). Re-examination of the data set measured at 215 K showed that although the systematic absence condition $h + k = 2n + 1$ was obeyed, except for two weak reflections, refinement in $Cmc2_1$ was not satisfactory, nor was the solution in $Pbc2_1$. However, by 205 K the systematic absence condition no longer held and refinement was possible in $Pbc2_1$. It is likely that the transformation to the primitive orthorhombic space group occurs close to 215 K, explaining the difficulty in refining the structure in either space group at this temperature. As a further detail, the average I/σ for the $h + k = 2n + 1$ class of reflections for the 100 K structure, for example, was 4.4 *versus* 9.75 for the whole data set. Of the total 13 900 independent reflections used in the refinement, 12 000 had $I > 2\sigma(I)$, very clearly showing that C-centring was no longer present. These average values are typical for the data sets below 205 K, marking the transition to the primitive orthorhombic unit cell. The fact that the $R_{\rm int}$ and conventional R values are generally higher for the $Pbc2_1$ crystal structures than for the other structures is explained by the weaker $h + k$ odd reflection subset.

All structures of (III) determined between 205 and 100 K were extremely well behaved in $Pbc2_1$ (see Figs. 2*k*, *l* and *m*); some degree of twinning was observed due to the similarity of a and b, but the disorder of the C13 and C25 atoms was no longer seen.

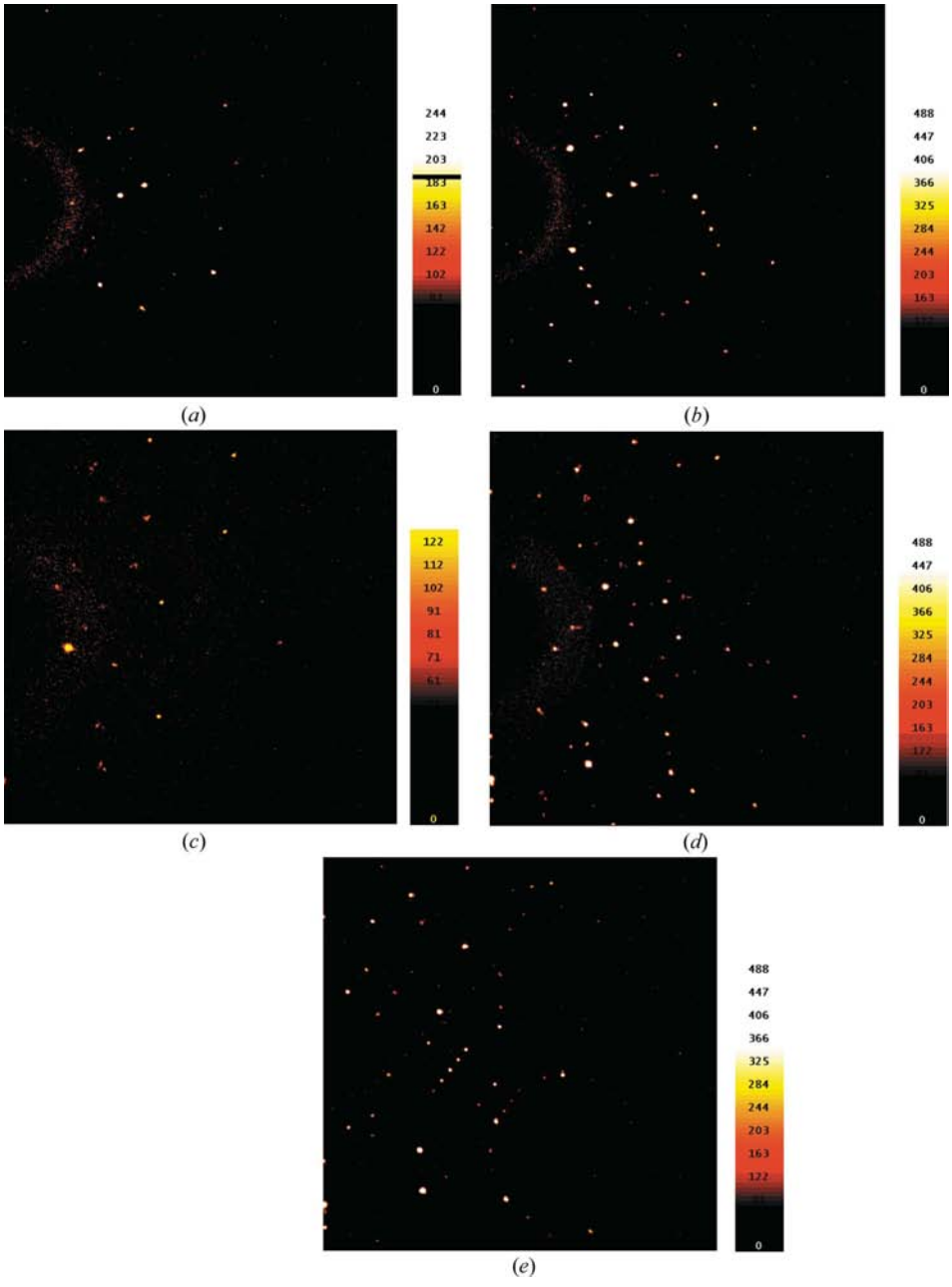

Figure 3
Diffraction patterns showing the differing lattice types at different temperatures [at identical setting for (*a*) and (*b*), and for (*c*), (*d*) and (*e*)]. (*a*) (I) at 293 K, showing the body-centred tetragonal lattice; (*b*) (I) at 230 K, where the lattice has become C-centred orthorhombic; (*c*) (III) at 260 K, showing the body-centred cubic lattice; (*d*) (III) at 230 K, where the lattice has become C-centred orthorhombic; (*e*) (III) at 205 K, where the lattice has become primitive orthorhombic.

3.2. Unit-cell parameters

3.2.1. (I) and (II). Plots of the unit-cell parameters are shown in the supplementary data [Figs. S1*a* and *b* for (I) and (II), respectively]; the tetragonal cells were transformed to cells equivalent to *C*-centred cells using the matrix (−1 −1 0/ 1 −1 0/ 0 0 1). For (I) the transition from tetragonal to *C*-centred leads to discontinuities in the reduction in the cell parameters seen as the temperature is lowered, which occur between 260 and 230 K. This is particularly marked for *a*, which reduces significantly more than *b*, and for *c*, which increases appreciably, due to the transition to the *C*-centred cell. The reduction in *a*, *b*, *c* and *V* is then steady from 230 to 95 K, with no obvious sign of a change around 100 K, which might be expected for the transition from $Cmc2_1$ to *Cc*.

For (II) again there are discontinuities between 260 and 230 K, and this is most obvious for *c*, which again increases slightly during the transition from tetragonal to *C*-centred; the similarity of *a* and *b*, even for the *C*-centred unit cells is obvious (Fig. S1*b*).

3.2.2. (III). Plots of the unit-cell parameters are shown for (III) in the supplementary data (Fig. S1*c*). The *a* parameter decreases and *b* increases, between 260 and 230 K, accompanying the transition from body-centred cubic to *C*-centred orthorhombic; then there is a sharp increase at 215 K, which is close to the probable transition temperature to the primitive orthorhombic cell. *c* and *V* show similar trends to one another, with significant reductions between 260 and 230 K accompanying the transition from cubic to C-centred orthorhombic. Then there is a further discontinuity at ∼ 215 K, marked by increases in *c* and *V*, arising from the transition to the primitive orthorhombic cell. A gradual reduction in all parameters takes place from 205 to 130 K, but there does seem to be a slight rise, particularly in *b*, between 130 and 100 K. This could signify further symmetry reduction, and the space groups *Pc* and $P2_1$ were investigated, but neither provided an improved model over the model in $Pbc2_1$.

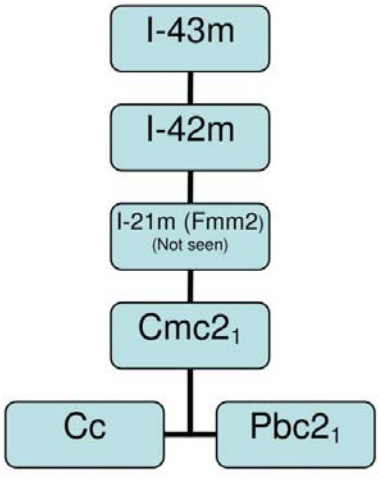

Figure 4
Relationship between the space groups seen for complexes (I), (II) and (III). Note that the space group $I\bar{2}1m$ is a non-standard setting of the space group *Fmm*2. This space group is not seen for any of the complexes, but it is the likely space group linking between $I\bar{4}2m$ and $Cmc2_1$.

4. Discussion

4.1. Space-group conversion pathways

The thermotropic behaviour observed as the temperature was reduced can be understood in terms of transitions down chains of maximal subgroups (*International Tables*, Vol. A, 1992, and the program *SYMMODES*; Capillas *et al.*, 2003); the space-group pathways for (I) and (II), are somewhat different, although related to that of (III), and these are shown in Fig. 4.

Complex (III) at 293 K exists in the space group $I\bar{4}3m$, whilst (I) and (II) have the space group $I\bar{4}2m$, which is a maximal subgroup of $I\bar{4}3m$ of type I and index 3. The reduction of symmetry arises from the loss of threefold point symmetry; the symmetry of the *M*-atom site which lies on the $\bar{4}3m$ special position in $I\bar{4}3m$ is reduced to $\bar{4}2m$ in the space group $I\bar{4}2m$; similarly, the symmetry of the *M*′ and P atom sites is reduced from 3*m* to *m*, and all other atoms, which lie on mirror planes in $I\bar{4}3m$, either remain on mirror planes or have their symmetry reduced to general positions.

The $I\bar{4}2m$ space group is not seen for (III), but at 230 K all three complexes are found in the orthorhombic space group $Cmc2_1$. The route to this space group is somewhat more complex, being accessible by several space-group pathways; the most direct is *via* the maximal subgroup $I\bar{2}1m$, which is equivalent to the orthorhombic space group *Fmm*2. The reduction in symmetry arises from the removal of the $\bar{4}$ point symmetry; the symmetry of the *M* atom position is reduced from $\bar{4}2m$ to *mm*2 and the atoms which lie on a mirror plane in $I\bar{4}2m$ may or may not have that symmetry reduced to general positions. Although the space group $I\bar{2}1m$ (*Fmm*2) is not seen for any of the complexes, one of its maximal subgroups of the type (II*a*), and index 2, is $Cmc2_1$. This change of space group causes the symmetry of the *M*-atom position to be reduced from *mm*2 to *m*, and atoms which lie on the *m* special positions may become general.

When the temperature is lowered still further, (III) transforms to the space group $Pbc2_1$, which is a maximal subgroup of $Cmc2_1$ of type (II*a*) and index 2. This space group is not seen for (I) and (II), but the space-group symmetry of complex (I) reduces to *Cc*, at 100 K, which is another maximal subgroup of $Cmc2_1$ of type I and index 2. In either case, the change of space group removes the mirror symmetry from those atoms lying on *m* special positions and all atom positions become general.

4.2. Description of the structures

The molecules are distorted triangular dodecahedra (Haigh, 1995), with four $[M'O_4]^-$ ions and four TBPO ligands placed alternately at the vertices. Selected bond lengths and angles are shown in Tables 4 and 5 for the complexes at 293, 230 and 100 K [except for those of (III) at 293 K, owing to the high degree of disorder of this structure]; other parameters for all the crystal structures have been deposited. For each molecule

Table 4
Selected bond lengths (Å).

	(I) at 293 K	(I) at 230 K	(I) at 100 K	(II) at 293 K	(II) at 230 K	(II) at 100 K	(III) at 230 K	(III) at 100 K
*M*1—O13	2.272 (10)	2.261 (8)	2.280 (7)	2.320 (11)	2.280 (15)	2.287 (12)	2.302 (8)	2.337 (9)
*M*1—O9	–	2.272 (8)	2.305 (8)	–	2.337 (15)	2.293 (11)	2.290 (9)	2.348 (8)
*M*1—O5	–	2.297 (6)	2.311 (11)	–	2.362 (11)	2.368 (8)	2.314 (7)	2.374 (8)
*M*1—O5*A*	–	2.297 (6)	2.305 (11)	–	2.362 (11)	2.368 (8)	2.313 (7)	2.368 (8)
*M*1—O10	2.411 (10)	2.396 (8)	2.434 (7)	2.436 (11)	2.462 (13)	2.454 (11)	2.438 (10)	2.437 (9)
*M*1—O6	–	2.404 (8)	2.426 (7)	–	2.489 (11)	2.461 (11)	2.398 (10)	2.444 (9)
*M*1—O1	–	2.428 (6)	2.440 (10)	–	2.489 (11)	2.464 (8)	2.433 (7)	2.465 (8)
*M*1—O1*A*	–	2.428 (6)	2.419 (10)	–	2.502 (14)	2.464 (8)	2.433 (7)	2.449 (8)
M′1—O2	–	1.667 (8)	1.675 (12)	–	1.681 (11)	1.693 (9)	1.613 (9)	1.691 (10)
M′1—O3	–	1.690 (8)	1.698 (13)	–	1.690 (11)	1.703 (9)	1.663 (9)	1.704 (10)
M′1—O4	–	1.700 (7)	1.798 (11)	–	1.715 (11)	1.711 (8)	1.672 (7)	1.683 (11)
M′1—O1	1.749 (10)	1.748 (6)	1.752 (11)	1.742 (12)	1.720 (11)	1.756 (9)	1.710 (7)	1.759 (9)
M′2—O8*A*	–	1.688 (7)	1.691 (12)	–	1.701 (12)	1.668 (9)	1.621 (8)	1.676 (10)
M′2—O8	–	1.688 (7)	1.697 (11)	–	1.701 (12)	1.668 (9)	1.621 (8)	1.703 (10)
M′2—O7	–	1.705 (10)	1.652 (12)	–	1.722 (13)	1.737 (11)	1.630 (10)	1.723 (10)
M′2—O6	–	1.770 (8)	1.757 (7)	–	1.761 (14)	1.743 (11)	1.752 (10)	1.750 (9)
M′3—O11*A*	–	1.646 (8)	1.676 (12)	–	1.550 (13)	1.660 (11)	1.603 (9)	1.670 (11)
M′3—O11	–	1.646 (8)	1.651 (11)	–	1.550 (13)	1.660 (11)	1.603 (9)	1.697 (10)
M′3—O12	–	1.675 (10)	1.689 (9)	–	1.706 (13)	1.691 (10)	1.626 (11)	1.706 (9)
M′3—O10	–	1.756 (8)	1.737 (7)	–	1.711 (13)	1.753 (10)	1.705 (10)	1.758 (10)
M′1*A*—O3*A*	–	–	1.667 (14)	–	–	–	–	1.683 (10)
M′1*A*—O2*A*	–	–	1.681 (12)	–	–	–	–	1.703 (9)
M′1*A*—O4*A*	–	–	1.724 (12)	–	–	–	–	1.671 (11)
M′1*A*—O1*A*	–	–	1.771 (11)	–	–	–	–	1.751 (9)
P1—O5	1.506 (11)	1.508 (6)	1.520 (11)	1.522 (12)	1.513 (11)	1.515 (8)	1.503 (7)	1.509 (9)
P2—O9	–	1.506 (9)	1.528 (8)	–	1.531 (15)	1.535 (12)	1.497 (11)	1.516 (9)
P3—O13	–	1.520 (8)	1.524 (8)	–	1.477 (16)	1.518 (12)	1.474 (9)	1.499 (10)
P1*A*—O5*A*	–	–	1.520 (11)	–	–	–	–	1.515 (8)

at the various temperatures, the bond lengths generally agree within experimental error, although for (III) there are several examples of slight differences in bond lengths between the structures at 230 and 100 K. The bond lengths around *M* [*M* = U for (I), and Th for (II) and (III)] fall into two groups, namely *M*—OTBPO and *M*—O*M*′ [*M*′ = Re for (I) and (II), and Tc for (III)]. For (I) the *M*—O bond lengths are slightly shorter than those found in complexes (II) and (III), reflecting the larger ionic radius of Th^{4+} *versus* U^{4+} (119 and 114 pm, respectively, for the eight coordinate M^{4+} ions; from http://www.webelements.com/webelements/elements/text/U/radii.html); for example, for the 100 K crystal structures (I) has average *M*—OTBPO bond distances of 2.302 (5) Å and *M*—O*M*′ of 2.421 (5) Å, whilst the same average distances for (II) are 2.329 (5) and 2.461 (5) Å, and for (III) are 2.356 (4) and 2.450 (4) Å, respectively. Re—O and Tc—O bond lengths also fall into two groups, *i.e.* those that arise from the terminal O atoms and those from the O atoms bonded to the central M atom, and overall the equivalent bond lengths agree for all three complexes within experimental error, reflecting the similar ionic radii of Re^{7+} and Tc^{7+} (52 and 51 pm, respectively, for the four coordinate M'^{7+} ions; from http://www.webelements.com/webelements/elements).

Looking at the bond angles about the central *M* atom (Table 5), for all the crystal structures in the space group $Cmc2_1$, in general, there is no significant difference between equivalent bond angles. Also, the agreement between these bond angles for (I) and (II) measured at all temperatures is reasonably close, even though there are one or two space-group transitions in the whole temperature range. However, there are major differences between the bond angles about *M* in (III) in the space $Pbc2_1$ and any of the other crystal structures, including that of (III) at 230 K, indicating that the space-group transition between $Cmc2_1$ and $Pbc2_1$ causes a major change in conformation of the molecule. In general, the particularly large differences are seen for the OTBPO—Th—OTBPO and OTc—Th—OTc bond angles, while the OTBPO—Th—OTc match reasonably closely with the equivalent angles of the other crystal structures. For example, the OTBPO—*M*—OTBPO angle, O9—*M*1—O13, varies from 133.6 (4) to 138.7 (6)° for all the structures from 293 to 100 K, except (III) at 100 K [also not including the disordered 293 K structure of (III)], whereas for (III) at 100 K the corresponding angle is 117.7 (4)° (Table 5). Similarly, the O*M*′—*M*—O*M*′ angle, O1*A*—*M*1—O1, varies from 76.5 (3) to 80.7 (4)° for all the structures except for (III) at 100 K, where the corresponding angle is 105.9 (3)°. This is in contrast to the OTBPO—*M*—O*M*′ angles, which show much smaller differences; for example, the O13—*M*1—O1*A* angle varies from 73.6 (3) to 74.1 (2)° for all the structures except (III) at 100 K, where this angle is 71.4 (3)°.

4.3. Comparison of the structures

The similarities and differences seen in geometric parameters are clarified further by comparison of the complexes using the program *OFIT* from the *SHELXTL* package (Bruker, 2001), where equivalent *M*, *M*′ and P atoms were fitted. Firstly, for (I) the r.m.s. deviation of these atoms between the 293 and 230 K structures was 0.043 Å, and it is clear from Fig. 5(*a*) that the heavy atoms are very well matched at the two different temperatures; most of the O

Table 5
Bond angles about *M* (°).

	(I) at 293 K	(I) at 230 K	(I) at 100 K	(II) at 293 K	(II) at 230 K	(II) at 100 K	(III) at 230 K	(III) at 100 K
O9—*M*1—O13	138.7 (6)	136.6 (4)	136.9 (3)	137.7 (3)	135.3 (6)	134.9 (5)	133.6 (4)	117.7 (4)
O9—*M*1—O5	97.1 (2)	98.88 (18)	103.2 (4)	97.7 (3)	100.2 (3)	100.1 (2)	99.49 (18)	127.2 (3)
O13—*M*1—O5	–	96.00 (18)	91.2 (4)	–	95.6 (3)	95.1 (2)	97.02 (18)	83.5 (3)
O9—*M*1—O5*A*	–	98.88 (18)	95.5 (4)	–	100.2 (3)	100.2 (2)	99.49 (18)	83.2 (3)
O13—*M*1—O5*A*	–	96.00 (18)	99.1 (4)	–	95.6 (3)	95.1 (2)	97.02 (18)	131.1 (3)
O5—*M*1—O5*A*	–	138.9 (3)	139.6 (3)	–	137.3 (6)	139.2 (4)	137.2 (4)	120.1 (3)
O9—*M*1—O6	71.6 (4)	70.6 (3)	70.1 (3)	70.8 (5)	70.9 (5)	71.3 (4)	71.8 (4)	73.4 (3)
O13—*M*1—O6	149.6 (4)	152.8 (3)	152.8 (3)	152.2 (5)	153.7 (5)	153.8 (4)	154.6 (4)	153.8 (3)
O5—*M*1—O6	74.1 (2)	75.76 (16)	77.5 (4)	73.9 (3)	76.0 (3)	76.8 (2)	75.04 (19)	71.7 (3)
O5*A*—*M*1—O6	–	75.76 (16)	75.7 (4)	–	76.0 (3)	76.8 (2)	75.04 (19)	71.3 (3)
O9—*M*1—O1*A*	–	72.2 (2)	72.7 (3)	–	72.3 (4)	71.3 (4)	71.1 (3)	74.5 (3)
O13—*M*1—O1*A*	–	74.1 (2)	73.6 (3)	–	73.7 (4)	74.1 (3)	73.8 (3)	71.4 (3)
O5—*M*1—O1*A*	–	149.0 (2)	147.3 (4)	–	151.0 (4)	148.6 (3)	151.6 (3)	153.3 (3)
O5*A*—*M*1—O1*A*	–	72.0 (2)	72.5 (4)	–	71.5 (4)	72.0 (3)	71.0 (3)	73.4 (3)
O9—*M*1—O1	–	72.2 (2)	72.7 (3)	–	72.3 (4)	70.9 (3)	71.1 (3)	70.3 (3)
O13—*M*1—O1	–	74.1 (2)	74.0 (3)	–	73.7 (4)	74.1 (3)	73.8 (3)	71.3 (3)
O5—*M*1—O1	–	72.0 (2)	71.5 (4)	–	71.5 (4)	72.0 (3)	71.0 (3)	73.1 (3)
O5*A*—*M*1—O1	–	149.0 (2)	148.9 (4)	–	151.0 (4)	148.6 (3)	151.6 (3)	152.2 (3)
O9—*M*1—O10	–	149.0 (3)	148.3 (3)	–	149.6 (5)	149.3 (4)	152.0 (4)	154.5 (3)
O13—*M*1—O10	–	74.4 (3)	74.7 (3)	–	75.1 (5)	75.8 (4)	74.6 (3)	75.5 (4)
O5—*M*1—O10	–	72.88 (16)	73.0 (4)	–	71.7 (3)	72.2 (2)	72.54 (18)	73.5 (3)
O5*A*—*M*1—O10	–	72.88 (16)	72.3 (4)	–	71.7 (3)	72.2 (2)	72.54 (18)	72.4 (3)
O6—*M*1—O10	78.0 (6)	78.4 (3)	78.4 (3)	81.4 (7)	78.7 (4)	78.0 (3)	79.9 (4)	104.6 (3)
O1*A*—*M*1—O10	127.1 (4)	129.2 (2)	127.3 (4)	125.1 (4)	128.3 (3)	130.2 (3)	127.6 (2)	91.1 (3)
O1—*M*1—O10	–	129.2 (2)	131.4 (4)	–	128.3 (3)	130.2 (3)	127.6 (2)	134.9 (3)
O6—*M*1—O1*A*	–	125.4 (2)	127.6 (4)	–	124.6 (3)	124.8 (3)	123.9 (2)	134.3 (3)
O6—*M*1—O1	–	125.4 (2)	123.6 (3)	–	124.6 (3)	124.8 (3)	12397 (2)	92.8 (3)
O1*A*—*M*1—O1	–	76.9 (3)	76.5 (3)	–	79.6 (5)	76.7 (4)	80.7 (4)	105.9 (3)

atoms fit fairly well, but there are some more significant deviations of the C atoms of the ^{n}Bu groups. Similar results were seen in comparing (II) at 293 and 230 K (r.m.s. deviation = 0.065 Å). The r.m.s. deviation of the 230 and 100 K structures of (I) was 0.090 Å (Fig. 5*b*) and it is clear that generally the lighter atoms fit reasonably closely, except in the disordered ^{n}Bu regions of the 230 K structure. The structures of (II) at 230 and 100 K are much more similar (r.m.s. deviation = 0.029 Å), with the main differences again found in the regions of disorder in the ^{n}Bu groups (Fig. 5*c*); since these two structures are both in $Cmc2_1$, their correspondence is to be expected. It was also found that different complexes in the same space group showed very close resemblance; for example, the r.m.s. deviation of structures (I) and (II) at 293 K was found to be 0.058 Å; similarly, all the structures at 230 K (in the space group $Cmc2_1$) match very closely, with the r.m.s. deviation of the structures of (I) and (II) of 0.055 Å, structures (I) and (III) 0.069 Å, and (II) and (III) 0.056 Å.

However, the structures of (III) at 293 and below 205 K (space groups $I\bar{4}3m$ and $Pbc2_1$, respectively) are both quite different from all the other structures, including the structure of (III) at 230 K; for example, comparing the *M*, *M*′ and P atoms of the structures of (III) at the different temperatures, between the 293 and 230 K structures, the r.m.s. deviation = 0.366 Å (Fig. 5*d*), and between the 230 and 100 K structures, the r.m.s. deviation = 0.399 Å (Fig. 5*e*); the r.m.s. deviation between the 293 and 100 K structures is slightly reduced to 0.279 Å showing that the Th, Tc and P atoms are a little better matched but due to the disorder of (III) at 293 K, the C and O atoms positions do not correspond well.

The crystal structures can also be evaluated by comparing their polyhedron plots, a selection of which are shown in Fig. 6; these show the central *M* atom as a dodecahedron, and the *M*′ and P atoms as tetrahedra, and the dodecahedron is linked to the tetrahedra by corner sharing; the variation of the four molecules contained in the C-centred and primitive unit cells seen at 230 K and below is displayed The 293 K structures of (III) and (II) in the space groups $I\bar{4}3m$ and $I\bar{4}2m$, respectively, show the high symmetry of these two structures (Figs. 6*a* and *b*). At 230 K each structure is found in the orthorhombic space group $Cmc2_1$, which is shown for (III) in Fig. 6(*c*). This shows some tilting of the polyhedra relative to one another, compared with those seen in Figs. 6(*a*) and (*b*). For (I), reduction of the temperature leads to the transition to *Cc*, as shown in Fig. 6(*d*), which shows only minor differences in tilt angles compared with Fig. 6(*c*). Finally, Fig. 6(*e*) shows (III) in the space group $Pbc2_1$, which has a much larger change in the relative tilt angles of the three different polyhedra types, illustrating the significant difference of this structure to all the others.

The changes of space group also lead to changes in the packing arrangement of the molecules. Firstly, there are adjustments of the distances between the central *M* atoms, which have 14 neighbours in the closest coordination shell. Fig. 7 shows the arrangement for (III) at 293 K. The distances are either 15.342 or 13.287 Å, between the six neighbours in the direction of the faces or eight neighbours towards the vertices of the cell, respectively; the former distance is the unit-cell dimension. Reduction of the symmetry leads to changes in these two distances. Firstly, in the direction of the

faces, the distances change from 15.342 Å to the ranges 14.736–15.212 Å at 230 K and 14.820–15.297 Å at 100 K, with the two shortest distances arising from the reduction of the *c* unit-cell dimension. Secondly, at the same time, the distances to the vertices change from 13.287 Å to the ranges 12.981–13.152 Å at 230 K and 12.948–13.357 Å at 100 K. Thus, the space-group transition to $Cmc2_1$ leads to an overall reduction in all these distances, but the transition to $Pbc2_1$ leads, in some cases, to small increases. For (I) and (II), the distances generally reduce with temperature; for example, for (I), the distances in the direction of the faces of the unit cell are in the range 14.819–15.540 Å at 293 K, 14.829–15.360 Å at 230 K and 14.784–15.229 Å at 100 K, and the distances to the vertices are 13.253 Å at 293 K, and in the range 13.071–13.285 Å at 230 K and 13.004–13.175 Å at 100 K.

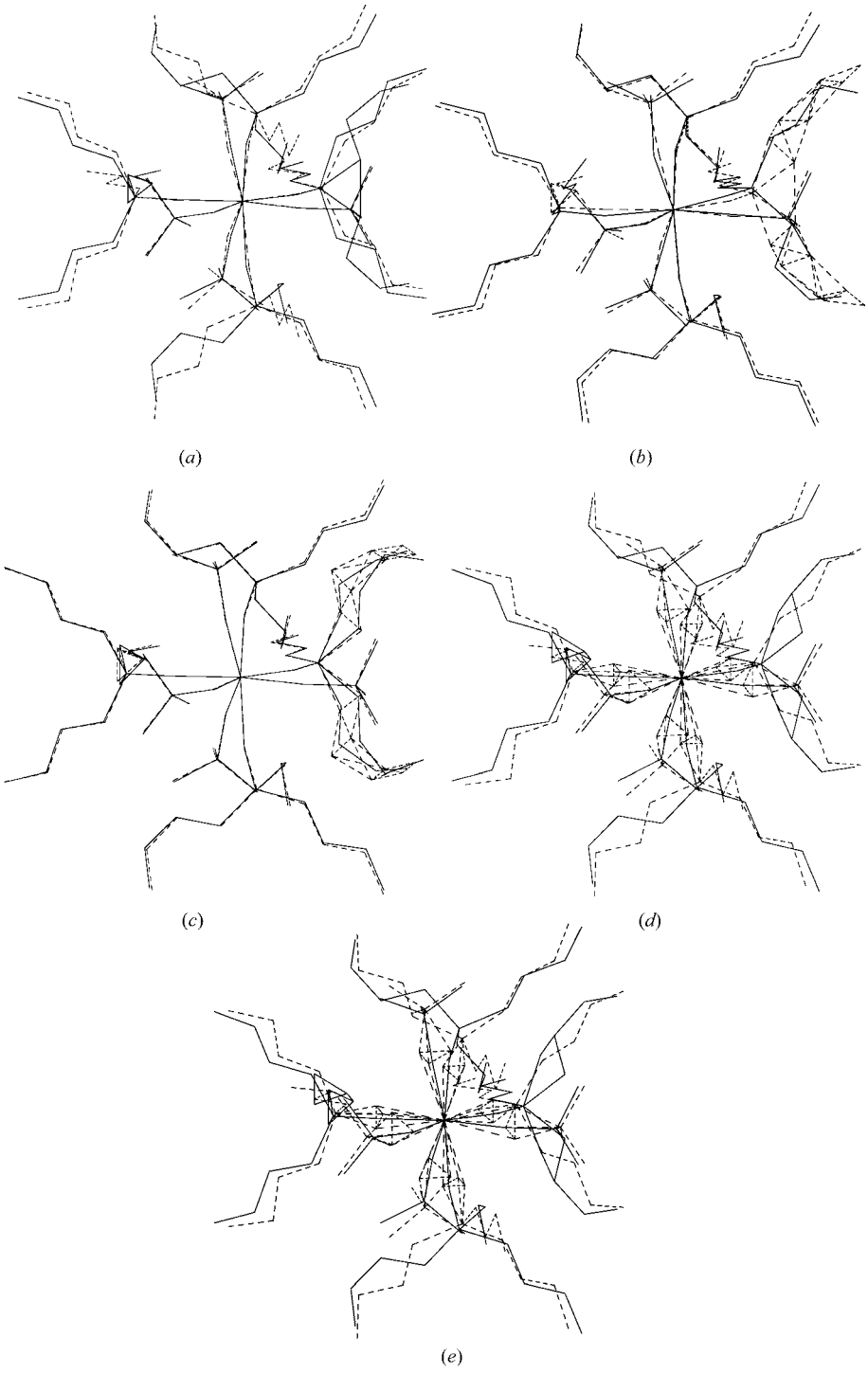

Figure 5
Comparison of the structures using the program *OFIT* from the *SHELTL* program suite (Bruker, 2001). The same view has been used as in Figs. 1 and 2. (*a*) Overlay of (I) at 293 K (dashed lines) and 230 K. (*b*) Overlay of (I) at 230 K (dashed lines) and 100 K. (*c*) Overlay of (II) at 230 K (dashed lines) and 100 K. (*d*) Overlay of (III) at 293 K (dashed lines) and 230 K. (*e*) Overlay of (III) at 230 K (dashed lines) and 100 K.

The molecules are arranged so that the $M'O_4^-$ groups point towards TBPO groups of adjacent molecules. This probably arises firstly because the $M'O_4$ groups do not protrude as far from the central *M* atom as the TBPO groups; the former distance is around 4.6–4.8 Å to the outer most O atoms, whilst the latter is between 6.5–9 Å to the furthest C atoms. Thus, the ^{n}Bu groups of one molecule fit into the cavity of the smaller $M'O_4$ group of the next molecule to provide the optimum filling of the space between the molecules (see Fig. 8). The ^{n}Bu groups form a layer around the $M'O_4$ groups and so this configuration allows stabilization owing to a possible network of 20–30 weak intermolecular C—H···O hydrogen bonds per molecule; these are marked by the many contacts of less than 4 Å, which are present between the ^{n}Bu C atoms and the terminal O atoms of the $M'O_4$ groups of the neighbouring molecules. In addition, there are

numerous (around 40 per molecule) intramolecular C···O contacts less than 4 Å, arising from the proximity of adjacent TBPO and $M'O_4$ groups in the alternate arrangement of the ligands about the central *M* atom. Determination of these hydrogen bonds was carried out for the crystal structures at 230 and 100 K; those at 293 K were omitted from this analysis owing to the uncertainty of the C atom and especially the H-atom positions of the structures at this temperature. For the crystal structures at 230 K and below the calculated position of the H atoms should be accurate, except for those of the methyl groups where the torsion angle may not be correct (see §2.5). Owing to the uncertainty specifically of the methyl H-atom positions, these structures would be excellent candidates for neutron crystal structure analyses to determine their H-atom position and therefore their hydrogen bonding, precisely in the presence of these very heavy elements.

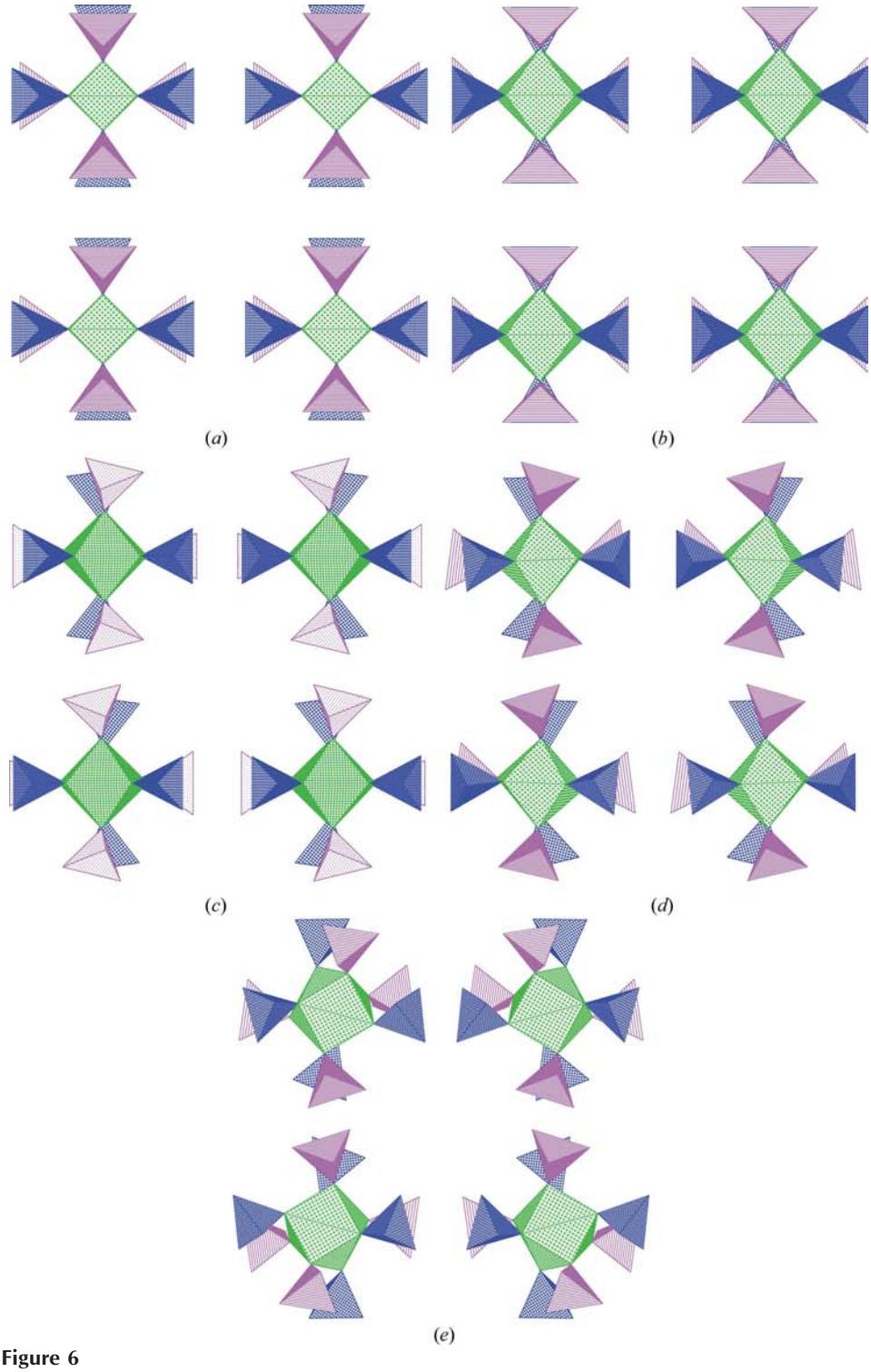

Figure 6
Polyhedron plots of the four molecules contained in the unit cells at 230 K and below, viewed down the *c* axis. The *M* atom is shown in green, *M′* in blue and P in purple; C atoms have been omitted for clarity. The plot for (III) at 293 K was prepared by using one component of the disordered O1 and O3 atoms. (*a*) (III) at 293 K; (*b*) (II) at 293 K; (*c*) (III) at 230 K; (*d*) (I) at 100 K; (*e*) (III) at 100 K.

Comparison of the hydrogen-bonding interactions revealed that they are very similar for all the cryostructures in the space group $Cmc2_1$, namely (I), (II) and (III) at 230 K, and (II) at 100 K. Also, the hydrogen bonding in (I) in the space group *Cc*, at 100 K, is closely comparable with the structures in $Cmc2_1$. However, because of the large differences of conformation between the structures of (III) at 230 and 100 K, there are also some differences in hydrogen bonding. There are other similar contacts where there is disorder of the ^{n}Bu chains at the higher temperature, but since these are less certain they will not be discussed here. The contacts for (III) at 230 and 100 K are listed in Table 6, between atoms where there is no disorder of the ^{n}Bu groups at the either temperature. Also, Fig. 9 shows the intermolecular hydrogen bonds between these atoms at the two temperatures, with differences arising from the changes in conformation at the two temperatures. Interaction cooperativity, where a number of hydrogen bonds work together, which appears to be the case for these complexes, tends to increase the strength of the hydrogen bonds to be greater than the sum of their individual energies (Desiraju, 1996; Desiraju & Steiner, 1999). Thus, it is very probable that these weak interactions influence both the way that

Table 6
Selected intra- and intermolecular hydrogen bonds for (III) at 100 and 230 K.

D—H···A	$d(D$—H)	d(H···A)	$d(D\cdots A)$	<(DHA)
(III) at 100 K				
C1—H1A···O11	0.99	2.83	3.696 (18)	147.0
C2—H2B···O5	0.99	2.85	3.265 (16)	105.7
C2—H2B···O6	0.99	2.90	3.578 (15)	126.7
C3—H3A···O(12)	0.99	2.77	3.602 (19)	142.5
C5—H5A···O2	0.99	2.73	3.614 (17)	148.8
C5—H5B···O6	0.99	2.49	3.230 (16)	131.6
C5—H5B···O8	0.99	2.79	3.736 (17)	160.3
C9—H9A···O2	0.99	2.84	3.689 (17)	144.1
C10—H10A···O11	0.99	2.62	3.318 (18)	127.3
C10—H10B···O4	0.99	2.87	3.608 (17)	132.3
C10—H10B···O5	0.99	2.85	3.179 (18)	100.3
C1A—H1C···O10	0.99	2.71	3.477 (15)	134.7
C1A—H1C···O12	0.99	2.60	3.549 (17)	160.8
C1A—H1D···O7	0.99	2.51	3.381 (16)	147.2
C5A—H5D···O7	0.99	2.81	3.612 (17)	139.0
C5A—H5D···O8A	0.99	2.99	3.606 (16)	121.2
C6A—H6C···O5A	0.99	2.97	3.262 (14)	98.2
C6A—H6C···O8A	0.99	2.87	3.557 (16)	127.3
C6A—H6D···O2A	0.99	2.70	3.363 (16)	124.3
C9A—H9D···O2A	0.99	2.78	3.690 (15)	152.6
C10A—H10C···O10	0.99	2.68	3.390 (15)	128.5
C10A—H10C···O1A	0.99	2.77	3.574 (15)	138.2
C10A—H10C···O5A	0.99	2.95	3.325 (14)	103.4
C1—H1B···O2^{i}	0.99	2.77	3.674 (17)	152.1
C6—H6B···O3^{i}	0.99	2.82	3.611 (16)	137.8
C4—H4A···O2^{i}	0.98	2.75	3.72 (2)	168.3
C12—H12B···O3^{i}	0.98	3.01	3.69 (2)	127.7
C9—H9B···O3^{i}	0.99	2.60	3.573 (17)	167.3
C12—H12C···O8^{ii}	0.98	2.76	3.697 (18)	160.0
C2A—H2C···O2A^{iii}	0.99	2.97	3.569 (16)	119.8
C2A—H2D···O4A^{iii}	0.99	2.79	3.645 (17)	145.4
C5A—H5C···O4A^{iii}	0.99	2.80	3.784 (16)	171.7
C12A—H12F···O3A^{iii}	0.98	2.69	3.552 (18)	146.4
C4A—H4E···O3A^{iv}	0.98	2.68	3.549 (17)	148.2
(III) at 230 K				
C2—H2A···O5	0.97	2.94	3.337 (14)	105.6
C2—H2A···O6	0.97	2.60	3.454 (14)	147.4
C2—H2A···O7	0.97	3.00	3.464 (16)	110.4
C2—H2A···O10	0.97	2.92	3.650 (16)	133.3
C3—H3B···O12	0.97	2.68	3.537 (19)	147.3
C5—H5B···O8	0.97	2.58	3.533 (14)	167.1
C5—H5A···O2	0.97	2.59	3.449 (14)	147.6
C9—H9A···O2	0.97	2.82	3.624 (15)	141.3
C9—H9A···O4	0.97	2.97	3.633 (14)	126.9
C10—H10A···O11	0.97	3.07	3.564 (16)	113.3
C10—H10B···O4	0.97	3.02	3.565 (15)	116.9
C10—H10B···O5	0.97	2.87	3.228 (14)	102.7
C4—H4A···O2^{v}	0.96	3.02	3.880 (19)	149.4
C6—H6B···O4^{v}	0.97	2.88	3.559 (13)	127.7
C6—H6A···O3^{v}	0.97	2.74	3.523 (13)	138.1
C9—H9B···O3^{v}	0.97	2.72	3.682 (13)	172.9

Symmetry codes: (i) $-x+1, -y, z+\frac{1}{2}$; (ii) $-x+1, y-\frac{1}{2}, z$; (iii) $-x, -y, z+\frac{1}{2}$; (iv) $x, y, z+1$; (v) $-x+\frac{1}{2}, -y+\frac{1}{2}, z+\frac{1}{2}$.

the molecules pack together and also their conformations at the different temperatures.

To summarize, all the crystal structures agree remarkably closely, except the structures of (III) at 293 K and those of (III) below 205 K, in the space groups $I\bar{4}3m$ and $Pbc2_1$, respectively. These two space groups are not seen for complexes (I) and (II). It is clear that as well as the possible increase of mobility, particularly of the ^{n}Bu groups as the temperature is increased, there is also an unexpected freedom of movement of the atoms bonded to the central M atom. This is indicated by the fact that some of the OTBPO—Th—OTBPO and OTc—Th—OTc bond angles in (III) differ by a surprising amount at different temperatures, and also illustrated by changes in the relative tilt angles of the linked polyhedra. Thus, the space-group transitions seen for (I) and (II) may be largely attributed to the altered degrees of mobility, especially of the ^{n}Bu groups. However, the much larger conformational changes seen for (III) presumably also

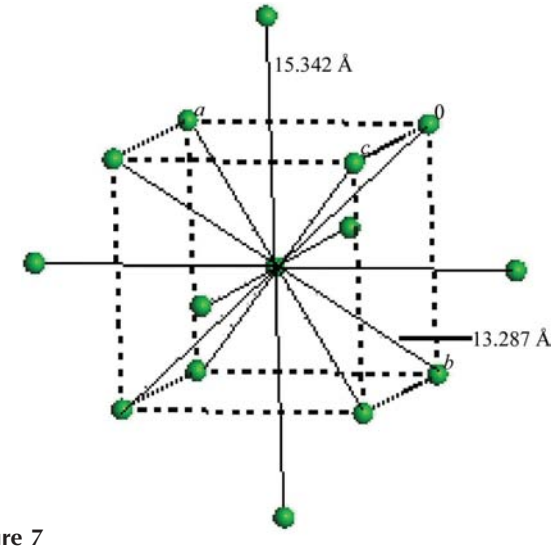

Figure 7
Packing arrangement for the central Th atom to its 14 nearest-neighbour Th atoms for (III) at 293 K, showing the body-centred cubic unit cell. The distances are either 15.342 or 13.287 Å between the neighbours in the direction of the faces or vertices of the cell, respectively.

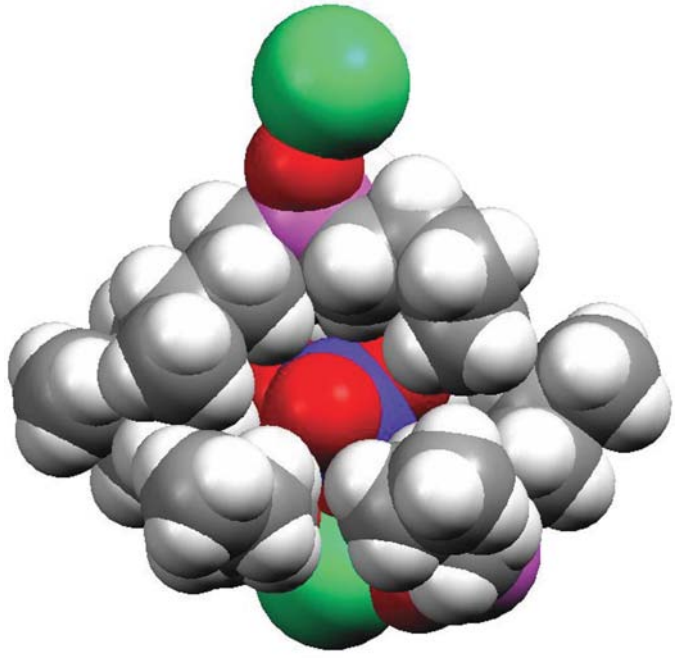

Figure 8
Space-filling diagram showing how the TBPO groups and [$M'O_4$] groups from adjacent molecules fit together (*MERCURY*; Bruno *et al.*, 2002).

arise from the differing packing constraints in the space groups $I\bar{4}3m$ and $Pbc2_1$.

The change of M from U in (I) to Th in (II), where M' is Re in each case, gives complexes that have very similar behaviour with temperature, although the ionic radius of Th^{4+} is somewhat larger than that of U^{4+}; however, the change of M' from Re in (II) to Tc in (III) causes a much greater alteration in the behaviour with temperature, even though the atomic radii of Tc^{7+} and Re^{7+} are similar, and the bond lengths about the M' atoms correspond very closely from structure to structure. Therefore, from a consideration of the bond lengths it is not clear why the apparently similar complex (III) shows this difference in behaviour compared with complexes (I) and (II). Also, a detailed study of the vibrational spectroscopy proved to be unhelpful; firstly, the $[TcO_4]^-$ stretches come at lower energy than the $[ReO_4]^-$ stretches and hence a direct comparison is impossible; secondly, for the TBPO ligand, the spectral features are almost identical for the three complexes, with the major P═O stretch coming at 1059, 1060 and 1057 cm^{-1}, respectively, for (I), (II) and (III). However, the different conformations and packing arrangements may be influenced by variations in the strength of the weak C—H···O intra- and intermolecular hydrogen-bonding interactions. These differences could in turn arise because of the possible variations in charge density on the O atoms of the pertechnetate ion *versus* the perrhenate ion; such differences in the basicity of the acceptor atoms would lead to variations in hydrogen-bond lengths and therefore strengths (Desiraju, 1996; Desiraju & Steiner, 1999).

Of particular interest in determining the reasons for the differing behaviour seen for (III) *versus* (I) and (II) would be to carry out temperature-resolved studies of the $[M(M'O_4)_4(TBPO)_4]$ structure, where M = U and M' = Tc, to find out whether its behaviour would be analogous to that of (I) and (II) or that of (III); unfortunately, the U^{4+} ion would be oxidized by pertechnetate, making the synthesis of this complex impossible. However, we intend to explore the chemistry of lanthanide analogues, which might show similar interesting behaviour with temperature and lead to greater insight into the causes for the variation in behaviour of these closely related complexes.

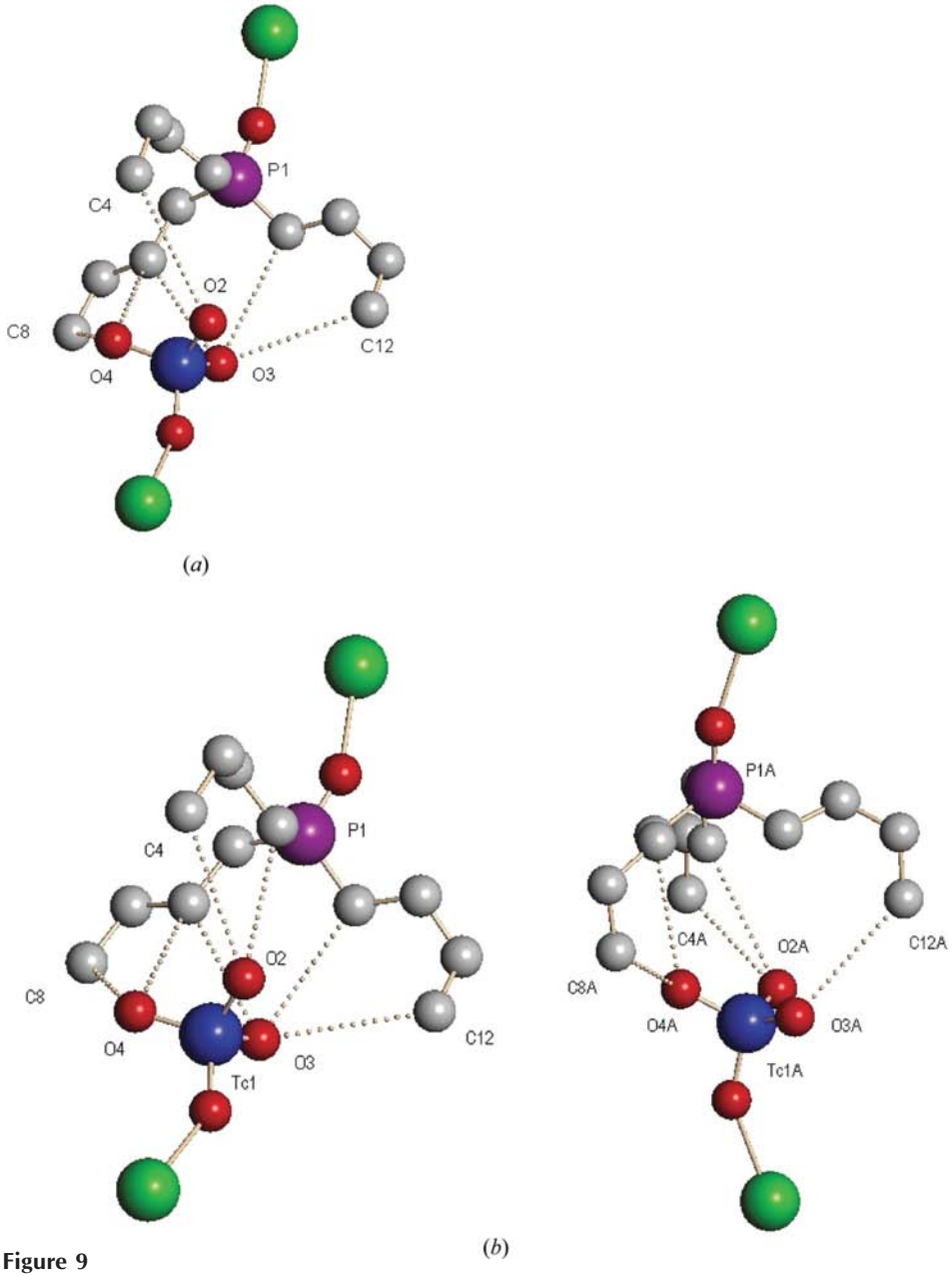

Figure 9
Comparison of the intermolecular C—H···O hydrogen-bonding interactions between C1—C12 and C1*A*—C12*A* and O1—O4 and O1*A*—O4*A* for (III) at (*a*) 230 K and (*b*) 100 K; note that at 230 K the two components, C1—C12 and C1*A*—C12*A*, and likewise O1—O4 and O1*A*—O4*A*, are related by mirror symmetry.

5. Conclusions

This ensemble of experiments demonstrates that for each complex the crystal structures show a stepwise improvement of order as the temperature is reduced, which is marked by changes of lattice centring and reduction of space-group symmetry. Liquid nitrogen cooling removes all or almost all the disorder seen at ambient temperature and it seems likely

that cooling to temperatures lower than 100 K might induce further phase transitions. In one case repetition of the experiment on two different diffractometers suggested a fine sensitivity to temperature setting close to the liquid nitrogen cryostream lower-temperature limit; in order to investigate this and any possible further space-group transitions, a liquid helium temperature facility would be required for future experiments. In addition, heat-capacity experiments using DSC would be helpful for investigating the space-group transitions.

The various results obtained suggest that firstly the freezing, particularly of the ^{n}Bu groups, which are highly mobile at 293 K, leads to space-group transitions as the temperature is reduced. Also, the constraints of the crystal packing for different space groups, together with the weak C—H···O hydrogen bonding, probably influence the overall geometry of these compounds and lead in some cases to some large changes of conformation between structures measured at different temperatures. We would expect that the changes are cooperatively intermolecular, although it is not possible to resolve whether the drive is enthalpic or entropic. The changes of the distances between the central *M* atoms of up to 0.6 Å represent a significant fraction of a hydrogen bond and must presumably affect the 25 to 30 intermolecular hydrogen bonds in each structure to a greater or lesser extent.

Finally, the formation of these complexes demonstrates that perrhenate and pertechnetate are sufficiently strong ligands to compete with TBPO and bind to actinide metal centres. Further studies are in progress to explore whether these complexes are stable in solution and therefore might be model complexes for species involved in the PUREX process.

References

Altomare, A., Burla, M. C., Camalli, M., Cascarano, G. L., Giacovazzo, C., Guagliardi, A., Moliterni, A. G. G., Polidori, G. & Spagna, R. (1999). *J. Appl. Cryst.* **32**, 115–119.

Bol'shakov, K. A., Sinitsyn, N. M., Travkin, V. F. & Borisov, V. V. (1967). *Dokl. Akad. Nauk SSSR*, **177**, 344–346.

Bruker (2001). *SMART*, Version 5.625, *SADABS*, Version 2.03*a*, and *SHELXTL*, Version 6.12. Bruker AXS Inc., Madison, Wisconsin, USA.

Bruker (2002). *SAINT*, Version 6.36*a*. Bruker AXS Inc., Madison, Wisconsin, USA.

Bruno, I. J., Cole, J. C., Edgington, P. R., Kessler, M., Macrae, C. F., McCabe, P., Pearson, J. & Taylor, R. (2002). *Acta Cryst.* B**58**, 389–397.

Capillas, C., Kroumova, E., Aroyo, M. I., Perez-Mato, J. M., Stokes, H. T. & Hatch, D. M. (2003). *J. Appl. Cryst.* **36**, 953–954.

Chakravorti, M. C. (1990). *Coord. Chem. Rev.* **106**, 205–225.

Desiraju, G. R. (1996). *Acc. Chem. Res.* **29**, 441–449.

Desiraju, G. R, & Steiner, T. (1999). *The Weak Hydrogen Bond in Structural Chemistry and Biology*, pp. 1–121. Oxford University Press.

Farrugia, L. J. (1999). *J. Appl. Cryst.* **32**, 837–838.

Fedosseev, A. M., Budantseva, N. A., Grigoriev, M. S., Guerman, K. E. & Krupa, J. C. (2003). *Radiochim. Acta*, **91**, 147–152.

Flack, H. D. (1983). *Acta Cryst.* A**39**, 876–881.

Haigh, C. W. (1995). *Polyhedron*, **14**, 2871–2878.

Herbst-Irmer, R. & Sheldrick, G. (1998). *Acta Cryst.* B**54**, 443–449.

John, G. H. (2003). PhD. Thesis. The University of Manchester, England.

John, G. H., May, I., Sarsfield, M. J., Steele, H. M., Collison, D., Helliwell, M. & McKinney, J. D. (2004). *Dalton Trans.* pp. 734–740.

Kenna, B. T. & Kuroda, P. K. (1961). *J. Inorg. Nucl. Chem.* **23**, 142–144.

Molecular Structure Corporation (1995). *TEXSAN*. MSC, 3200 Research Forest Drive, The Woodlands, TX 77381, USA.

Nardelli, M. (1995). *J. Appl. Cryst.* **28**, 659.

Otwinowski, Z. (1988). *DENZO*. Department of Molecular Biophysics and Biochemistry, Yale University, New Haven, Connecticut.

Parsons, S. (2003). *Acta Cryst.* D**59**, 1995–2003.

Sarsfield, M. J., Sutton, A. D., May, I., John, G. H., Sharrad, C. & Helliwell, M. (2004). *Chem. Commun.* pp. 2320–2321.

Sheldrick, G. M. (1997). *SHELX*97. University of Göttingen, Germany.

Sheldrick, G. M. (2002). *TWINABS*. Bruker-AXS, Madison, Wisconsin, USA.

Spek, A. L. (2003). *J. Appl. Cryst.* **36**, 7–13.

Sutton, A. D. (2003). PhD. Thesis. The University of Manchester, England.

Wilson, P. D. (1996). Editor. *The Nuclear Fuel Cycle*, pp. 116–183. BNFL plc, Oxford University Press.